DOE-HTGR-88510
Revision 0

ANALYSIS OF CAPSULE HFR-B1 GRAPHITE-CORROSION DATA

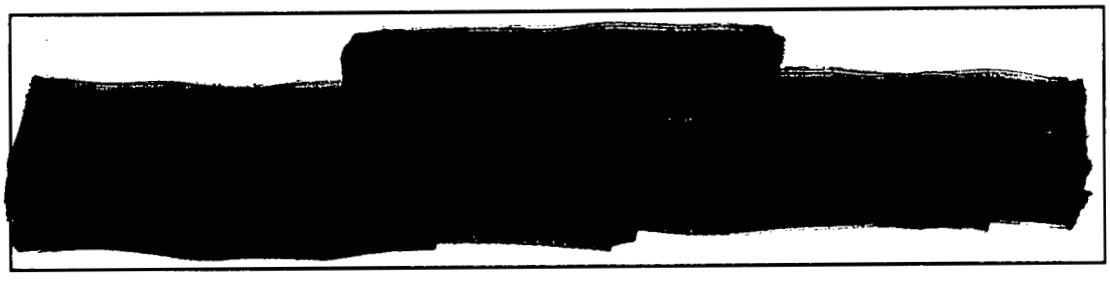

AUTHORS/CONTRACTORS

GENERAL ATOMICS

ISSUED BY GENERAL ATOMICS
FOR THE DEPARTMENT OF ENERGY
CONTRACT DE-AC03-89SF17885

JANUARY 1991

DISCLAIMER

DOE-HTGR-88510
Revision 0

CAUTION

Do not publicly release this document.

This technical report is being transmitted in advance of DOE patent clearance and no further dissemination or publication shall be made of the report without prior approval of the DOE Patent Counsel.

This document will be returned upon request or when no longer needed, unless notification has been received that this document has been cleared for release or publication.

PATCL 9/9/91

ANALYSIS OF CAPSULE HFT-B1 GRAPHITE-CORROSION DATA

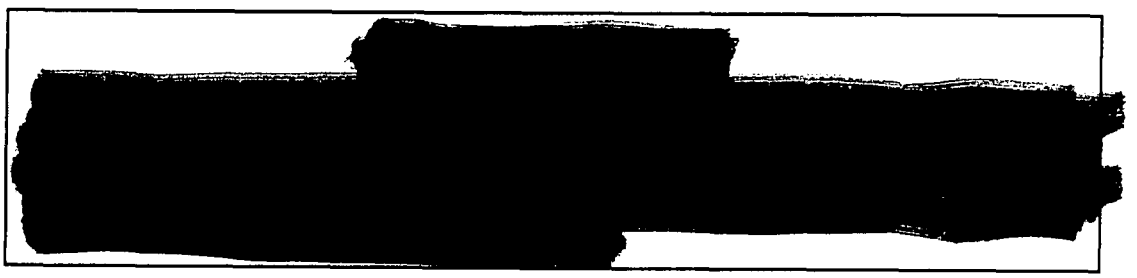

DISTRIBUTION OF THIS DOCUMENT IS UNLIMITED

This document is
PUBLICLY RELEASABLE
PER MEMO - DAVID A. STEINMAN, GENERAL ATOMICS CLASSIFICATION OFFICER, 1/23/01
Helen Allen

Issued By:
General Atomics
P.O. Box 85608
San Diego, California 92186-9784

DOE CONTRACT DE-AC03-89SF17885

GA Project 6300

JANUARY 1991

GENERAL ATOMICS

GA 1485 (REV. 9/89) R011 2225 **ISSUE/RELEASE SUMMARY**

☒ R&D ☐ DV&S ☐ RELEASE	APPVL LEVEL	DISC.	QA LEVEL	SAFETY	SYS	DOC. TYPE	PROJECT	DOCUMENT NO.	REV
			NA	NA					
	2	0	SEISMIC NA	ELECTRICAL NA	11	RGE	6300	DOE-HTGR-88510	0

TITLE:

ANALYSIS OF CAPSULE HFR-B1 GRAPHITE-CORROSION DATA

CM APPROVAL/ DATE	REV	PREPARED BY	APPROVAL(S) ENGINEERING	APPROVAL(S) QA	APPROVAL(S) PROJECT	REVISION DESCRIPTION/ W.O. NO.
INFO 3 JAN 2 2 1991	0	M.B. Richards 9/19/90 M.B. Richards; A.G. Gillespie 9/19/90 A.G. Gillespie	R.F. Turner 9/25/90 R.F. Turner		F.S. Ople	Initial Issue 7616012001 WBS 1601.2

CONTINUE ON GA FORM 1485-1

*See List of Effective Pages

NEXT INDENTURED DOCUMENT(S)

HTGR-86084

☐ GA PROPRIETARY INFORMATION

☒ NO GA PROPRIETARY INFORMATION

LIST OF EFFECTIVE PAGES

Page Number	Page Count	Revision
i through vi	6	0
1-1	1	0
2-1 through 2-3	3	0
3-1 through 3-21	21	0
4-1 through 4-9	9	0
5-1	1	0
6-1 through 6-2	2	0
A-1 through A-6	6	0
B-1 through B-11	11	0
Total Pages	60	

CONTENTS

FIGURES

TABLES

NOMENCLATURE

Symbols

d	diameter
P_{H_2O}	partial pressure of water vapor
R_1	inner radius of hollow cylinder of graphite
R_2	outer radius of hollow cylinder of graphite
$\rho_{C,o}$	initial graphite density
$A_{BET,o}$	initial BET surface area
ψ_o	structural parameter used to calculate the burnoff factor
Pe	Peclet number

Abbreviations

CEA	Commissariat a L'Energie Atomique
DDN	Design Data Needs
DOE	Department of Energy
dtf	designed to fail
EPA	Environmental Protection Agency
FIMA	fissions per initial metal atom
GA	General Atomics
JRC	Joint Research Center
KFA	Kernforschungsanlage
MHTGR	Modular High-Temperature Gas-cooled Reactor
ORNL	Oak Ridge National Laboratory
PIE	post-irradiation examination
ppmv	parts per million-vapor

1. SUMMARY

The recently completed irradiation of capsule HFR-B1 in the high-flux reactor at the Petten Establishment in The Netherlands provided some excellent data for fission-product release. The data were obtained under irradiation and temperature conditions close to those expected during normal operation of the Modular High-Temperature Gas-cooled Reactor (MHTGR). Some of the tests at Petten were designed to measure release of fission gases during hydrolysis of failed fuel. Hydrolysis was initiated by injecting known amounts of water vapor into the capsule sweep gas. The measured concentrations of CO and CO_2 in the capsule sweep gas indicated that a non-negligible amount of graphite corrosion was also occurring during the hydrolysis tests. Hence, these measurements provide some unique data for in-pile corrosion of grade H-451 graphite by steam.

In the present report, an analysis of graphite corrosion during the Petten hydrolysis tests is described. The calculations were performed using the REACT program, which is based on an improved corrosion model. The REACT program was developed as part of a research program at the University of California, San Diego, and is in operational status in the General Atomics (GA) Production Code Library. Predictions obtained with REACT show excellent agreement with the Petten graphite-corrosion data. Some small discrepancies are likely caused by reactions occurring within the fuel compacts, which are not presently modeled in REACT. This good agreement indicates that the currently used correlation for the steam-graphite reaction rate, which was obtained from out-of-pile measurements, may also be used to predict in-pile corrosion with good accuracy. This successful validation of REACT is a strong justification for further development of REACT to include the chemical-reaction and mass-transfer processes (including fuel hydrolysis) that occur within the fuel compacts.

2. INTRODUCTION AND BACKGROUND

Two important issues that affect the design of the MHTGR are (1) corrosion of fuel-element, reflector, and core-support graphite and (2) hydrolysis of defective or failed particles. In reference to the first issue, graphite structural integrity must be maintained for the loads and oxidant concentrations experienced during both normal operation and accident conditions. For economical plant operation, graphite corrosion must not impact the normal fuel-element replacement schedule and must not be the cause of extended reactor-shutdown periods.

The second issue is directly related to plant safety. During fuel hydrolysis, water vapor reacts with exposed fuel kernels to release gaseous and volatile fission products that have been stored in the kernel void space. For accidents that involve ingress of water or steam into the core, the increases in fisson-product release caused by hydrolysis must not result in violation of the Environmental Protection Agency (EPA) Protective Action Guidelines or the User/Utility Requirements. For the MHTGR fuel elements, graphite corrosion and fuel hydrolysis are inherently coupled; the water vapor must first penetrate a web of graphite before reaching the fuel compacts that contain the small fraction of failed and defective particles.

To ensure that the plant-design requirements are satisfied, mechanistic models have been developed to estimate graphite corrosion and fuel hydrolysis in the MHTGR. These models have been incorporated into the computer codes SURVEY/HYDROBURN (Ref. 1), OXIDE-3 (Ref. 2), and GOP (Ref. 3) that have been used for MHTGR design and safety analyses. In general, satisfactory agreement between current computer-code calculations of corrosion and data obtained from integrated experiments that

involve both transport and reaction phenomena had not been obtained previously. This lack of code validation results from approximations used in developing the mechanistic models, lack of sufficient data to accurately estimate model parameters, and possible misinterpretations of experimental results. The impact of using nonvalidated computer codes for plant design can be enormous. Without validated models, conservative calculations must be performed that may result in prohibitively high capital costs in order to meet plant-design requirements.

In order to improve the data base and understanding of graphite corrosion and fuel hydrolysis, technology development programs have been established under the Department of Energy (DOE) sponsored MHTGR program. Under these programs, experimental research is performed in order to satisfy Design Data Needs (DDNs) identified during a systematic analysis (formally referred to as Functional Analysis) of the plant design. In the United States, most of the MHTGR technology-development work is performed at Oak Ridge National Laboratory (ORNL). Additional experimental data is obtained from technology exchange agreements with foreign institutions, including the German national laboratory, Kernforschungsanlage (KFA) and the French Atomic Energy Commission, Commissariat a L'Energie Atomique (CEA).

Under representative MHTGR normal operating and accident conditions, very little experimental data exist for corrosion of grade H-451 graphite and hydrolysis of failed UCO fuel particles. For the coupled corrosion and hydrolysis processes, the only available data were obtained from the irradiations of capsule HRB-17 at ORNL (Ref. 4) and capsule HFR-B1 at the Petten Establishment in The Netherlands (Ref. 5). In these experiments, the loss of graphite mass as a function of time can be estimated from the measured concentrations of CO and CO_2 in the gas exiting the capsule. However, the only successful measurements for CO and CO_2 concentrations were obtained during the Petten experiment.

The Petten experiment was a cooperative program involving GA, KFA, ORNL, and the Petten Establishment of the Joint Research Center (JRC). The experiment was performed under the auspices of the US/FRG Umbrella Agreement for Cooperation in Gas-cooled Reactor Development. The primary purpose of the experiment was to obtain data for fission-gas release from failed fuel under both dry conditions and during fuel hydrolysis, and to obtain data for transport of metallic fission products in fuel compacts and graphite. The capsule geometry, temperature, and irradiation conditions were similar to those expected during normal operation of the MHTGR. The capsule irradiation lasted 445 full-power days and ended on July 10, 1989.

Although obtaining data for graphite corrosion was not a primary goal of the Petten experiment, the fuel compacts were housed within a graphite body, and graphite corrosion did occur during the fuel-hydrolysis experiments. Hence, the experiment provided data for the coupled processes of graphite corrosion and fuel hydrolysis under representative reactor conditions. The data may be used to partially satisfy DDNs M.10.01, "Validation of Design Methods for Graphite Corrosion," and M.07.12, "Data for Validation of Fission Gas Release" (see Ref. 6 for a description of DDNs). As described in Ref. 5, the estimated loss in graphite mass showed reasonable agreement with approximate hand calculations for graphite corrosion. The purpose of the present analysis is to perform a more detailed evaluation of the Petten graphite-corrosion data and to use the data to validate an improved graphite-corrosion model. Also, this analysis is a logical first step to understanding and modeling the complex phenomena that occur during fuel hydrolysis under reactor conditions.

The following sections describe the experimental data, model predictions, and conclusions drawn from this analysis. Two appendices are also included. Appendix A provides a detailed description of the graphite-corrosion model in the REACT program, which was used to simulate the Petten conditions. Sample REACT output is provided in Appendix B.

3. EXPERIMENTAL DATA

As shown in Fig. 1, the HFR-B1 capsule actually consisted of three separate capsules that were housed in a singular container, each with independent sweep-gas lines and temperature-control devices. Each capsule contained twelve fuel compacts in a cylindrical H-451 graphite body. The primary function for each capsule was to obtain data for fission-product release under irradiation conditions near to that expected in the MHTGR. To obtain statistically meaningful data, approximately 9% of the UCO particles in the fuel compacts were designed-to-fail (dtf) particles. In place of the normal TRISO coating, the fuel kernels for dtf particles were coated with only a single thin (20-30 μm) layer of pyrocarbon. These layers failed early in the irradiation to provide an adequate source of fission products. From capsule 1, fission-gas release data were obtained at near-isothermal conditions for temperatures in the range of 880° to 992°C. The effects of temperature cycling were studied in capsule 2, and the temperatures were varied from 880-1230°C. Of interest for the present application is the data obtained from capsule 3, in which water vapor was injected on sixteen separate occasions. The estimated burnups of fissile fuel were 18.3, 18.4, and 16.7% FIMA (fissions per initial metal atom) in capsules 1, 2, and 3, respectively.

Cross-sectional views of the capsule 3 geometry are shown in Fig. 2. The arrangement of fuel compacts and coolant holes is similar to that for the MHTGR fuel element. However, during the experiment, helium coolant did not flow through the coolant holes shown in Fig. 2. Instead, so-called piggyback samples, which consisted of unbonded fuel particles, encapsulated particles, and various non-fueled samples occupied the space in the central hole and in the coolant holes in order to satisfy other test objectives. The sweep-gas, which consisted of helium, injected impurities, and sometimes neon (for temperature

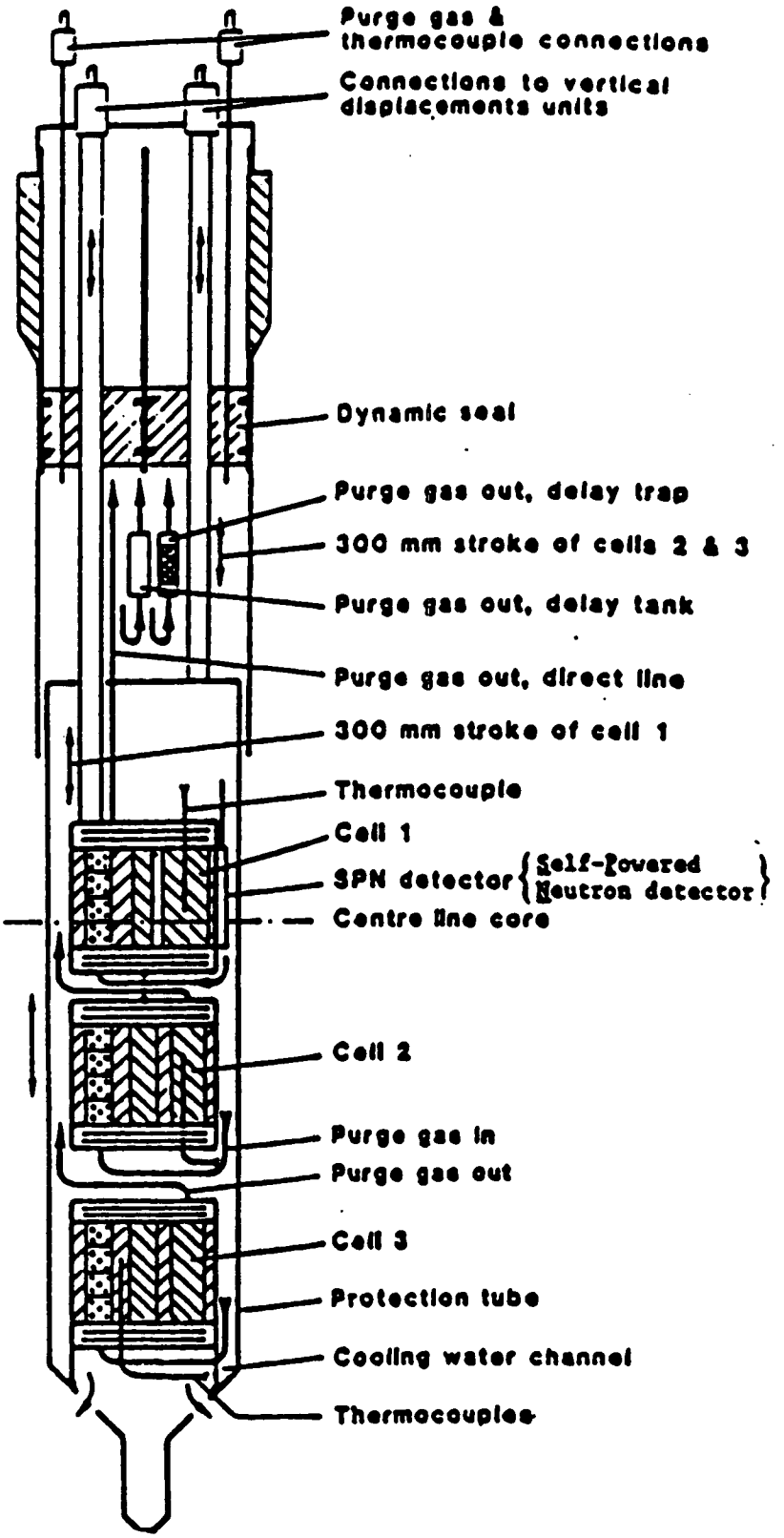

Fig. 1. Schematic of the HFR-B1 irradiation rig. The fuel-hydrolysis and graphite-corrosion data were obtained from capsule 3. This figure is taken from Ref. 2.

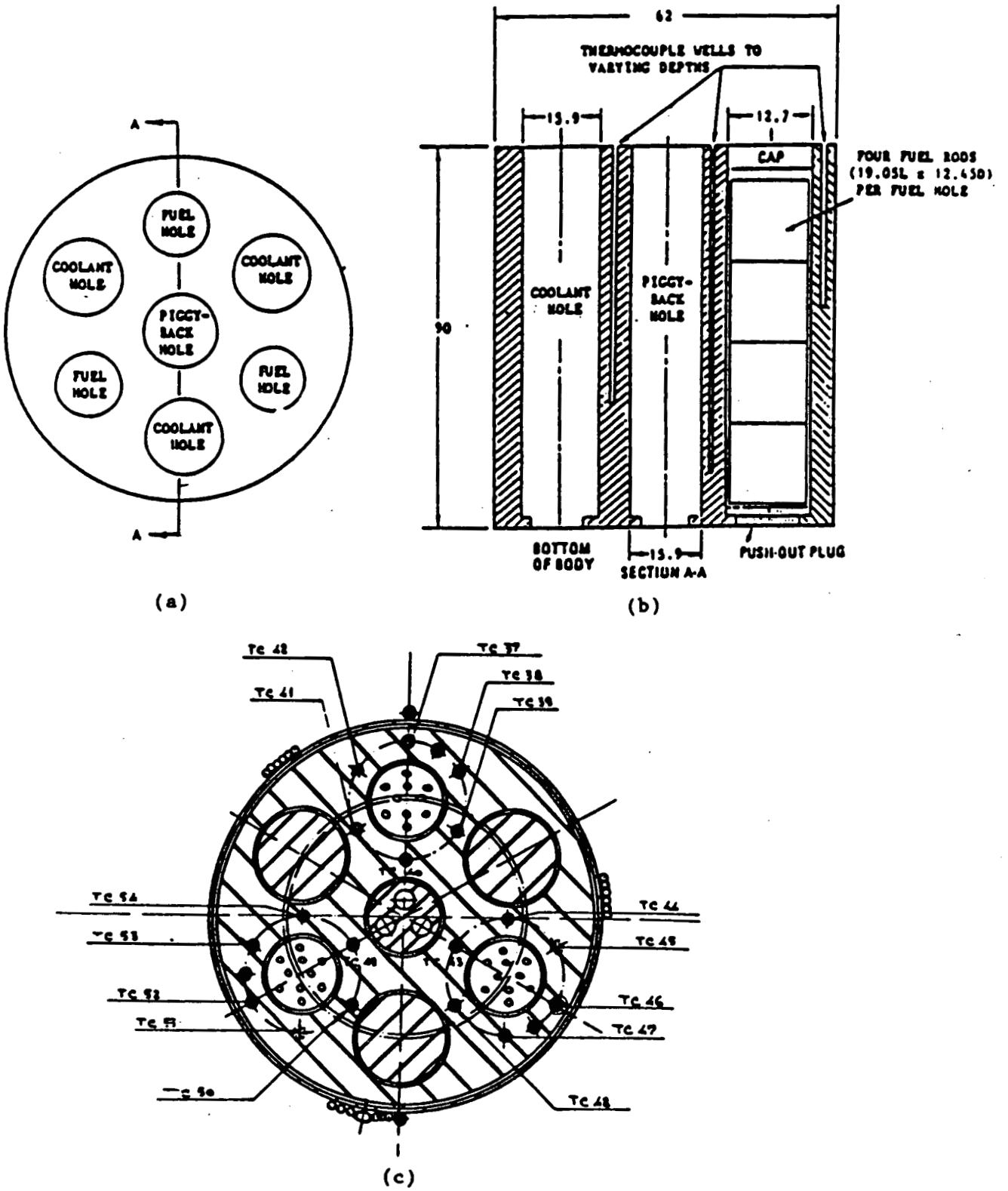

Fig. 2. Graphite body of capsule 3. (a) Top view of the capsule. (b) Side view of the capsule. (c) Top view showing thermocouple locations. Note that the thermocouples were positioned around the fuel compacts. The dimensions given are in millimeters. This figure was taken from Ref. 2

control), flowed between the outside of the graphite body with diameter d = 6.2 cm and the inside of the stainless steel shield containing the capsule with d = 7.4 cm. Thus, the transport paths of the water vapor, reaction-product gases, and fission gases differed from that in a representative MHTGR fuel element. However, the irradiation and temperature conditions were very similar to that expected in the MHTGR during normal operation (see Table 1).

During the sixteen injections, the water-vapor concentration was varied from 180 to 10,600 μatm. The graphite temperatures were measured with 18 thermocouples, the locations for which are shown in Fig. 2c. A numerical average of the 18 thermocouples resulted in temperatures varying from 670 to 900°C. The fuel-compact temperatures were not directly measured, but estimated from heat-transfer calculations. Based on these calculations, the fuel-compact temperatures were approximately 150°C higher than the average of the graphite-thermocouple measurements. The sweep-gas pressure was maintained at 3.6 atm and the mass-flow rate was about 0.83 mg/s (Reynolds No. $\simeq$ 0.2), with slight variations resulting from temperature changes.

A gas chromatograph was used to measure the concentrations of CO, CO_2, H_2, N_2, CH_4, and H_2O in the gas exiting the capsule. Figures 3 through 16 show the measured data for CO, CO_2, CH_4, and H_2, as well as the inlet-H_2O concentrations and the time periods for injection. The temperatures given in Figs. 3 through 16 refer to the calculated fuel-compact temperatures.

Since the CO and CO_2 result almost entirely from graphite corrosion, then the measured CO and CO_2 concentrations may be used to estimate the loss in graphite mass as a function of time. For the thermodynamic conditions in the Petten reactor, the likely reaction for steam-graphite corrosion is given by

$$C + H_2O \rightarrow CO + H_2 \quad . \qquad (1)$$

Table 1
Comparison of HFR–B1 and MHTGR Operating Conditions

Parameter	Units	HFR–B1		MHTGR	
		Target Level	Actual Operation	Normal Operation	Core Conduction Cooldown (1)
Peak Fast Fluence	10E+25 n/m~2	5.0	6.8	5.0	5.0
Peak Fiss. Burnup	% FIMA	22.0	18.5	26.0	26.0
Peak Fert. Burnup	% FIMA	3.0	5.0	4.0	4.0
Fuel Temp	C	850 – 1050	820 – 1050	700 – 1250	900–1620
Helium Gas Press.	atm	3.0	3.6	63	1 – 63
Helium Gas Flow Rate	cm~3/min	300	300	1.19E+5	small

(1) The ranges for values include both pressurized and depressurized conditions.

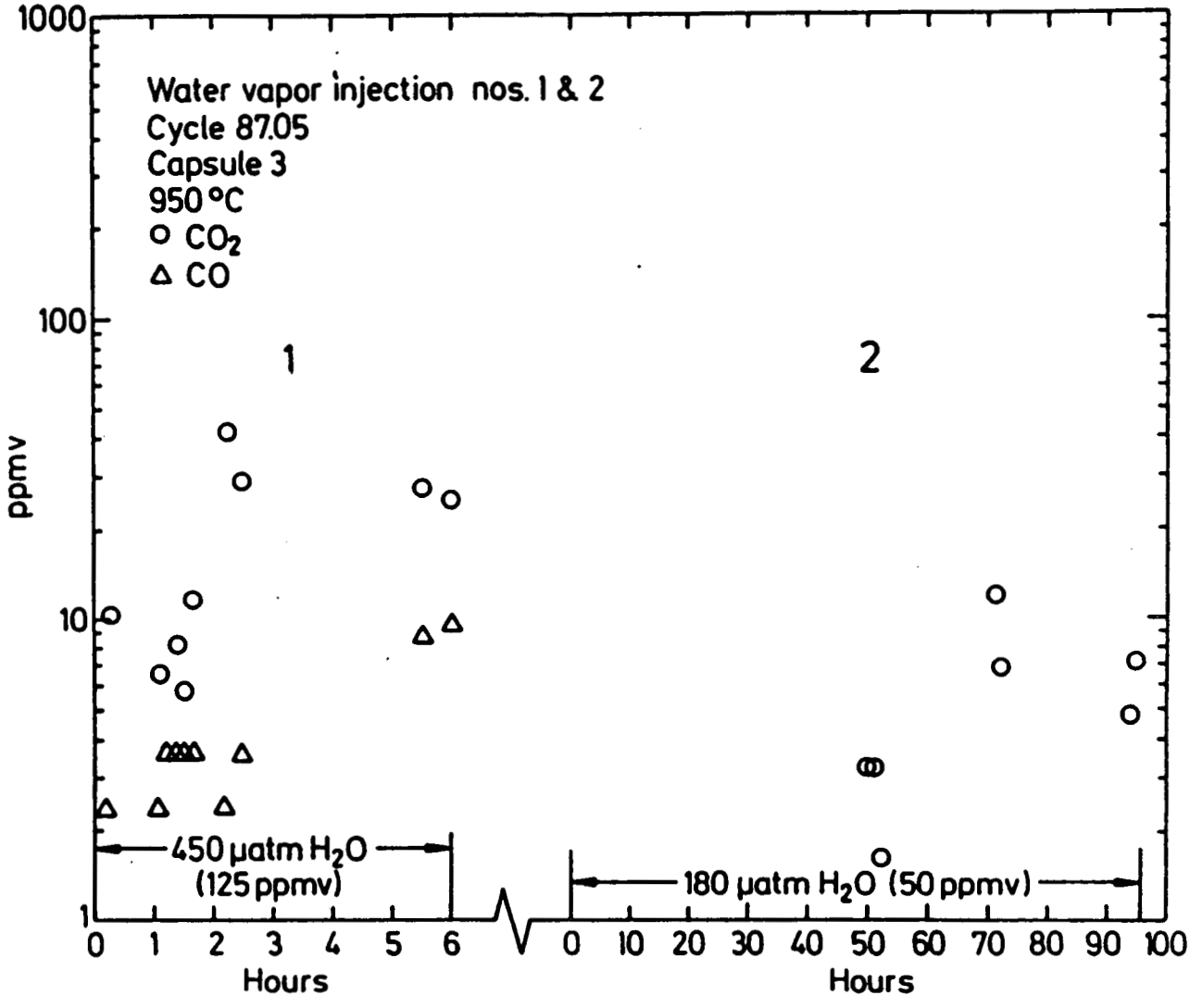

Fig. 3. Gas-impurity data during water-vapor injections Nos. 1 and 2. The temperature given refers to the fuel compacts. The water-vapor concentrations are inlet values. This figure is taken from Ref. 2.

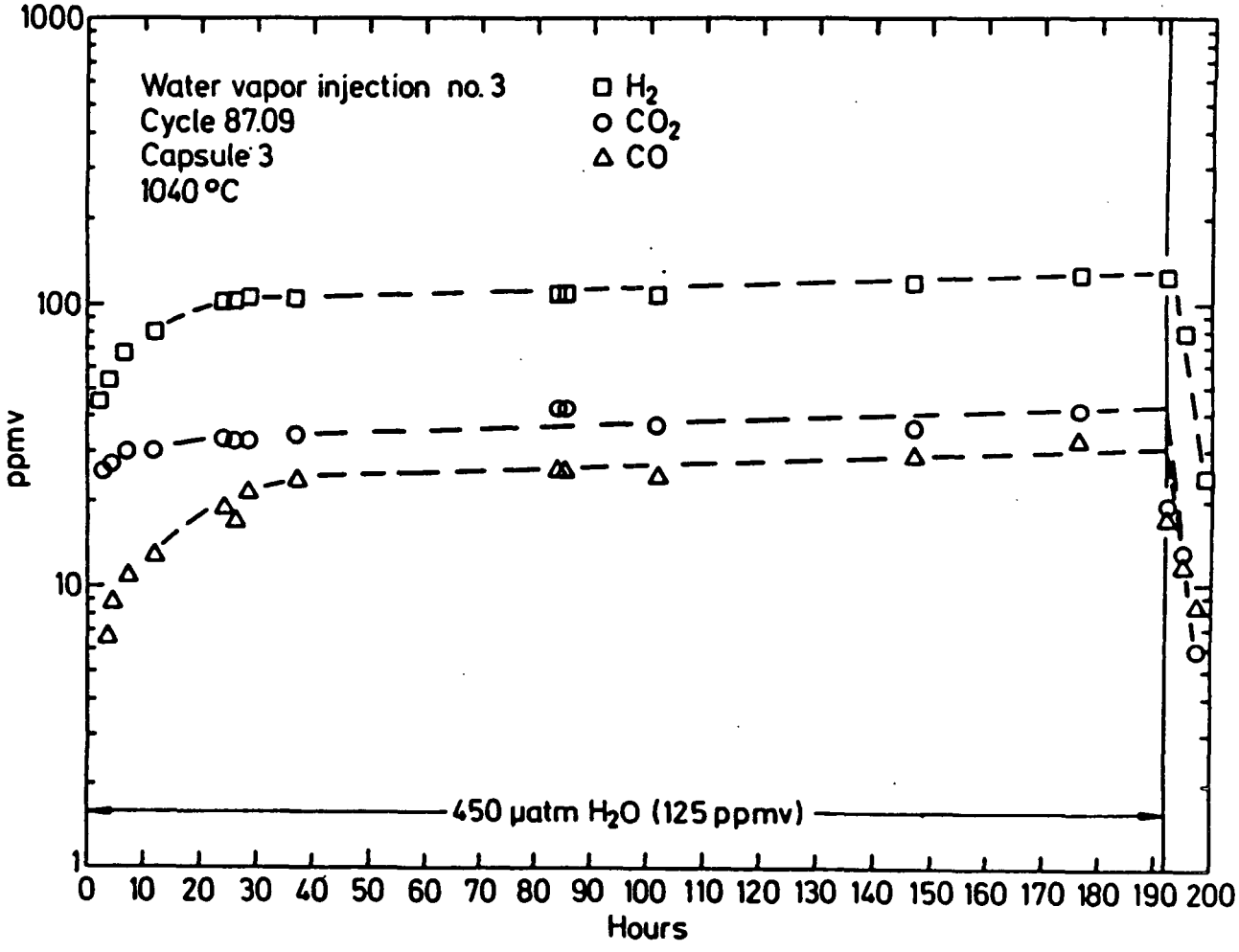

Fig. 4. Gas-impurity data during water-vapor injection No. 3. The temperature given refers to the fuel compacts. The water-vapor concentration is the inlet value. This figure is taken from Ref. 2.

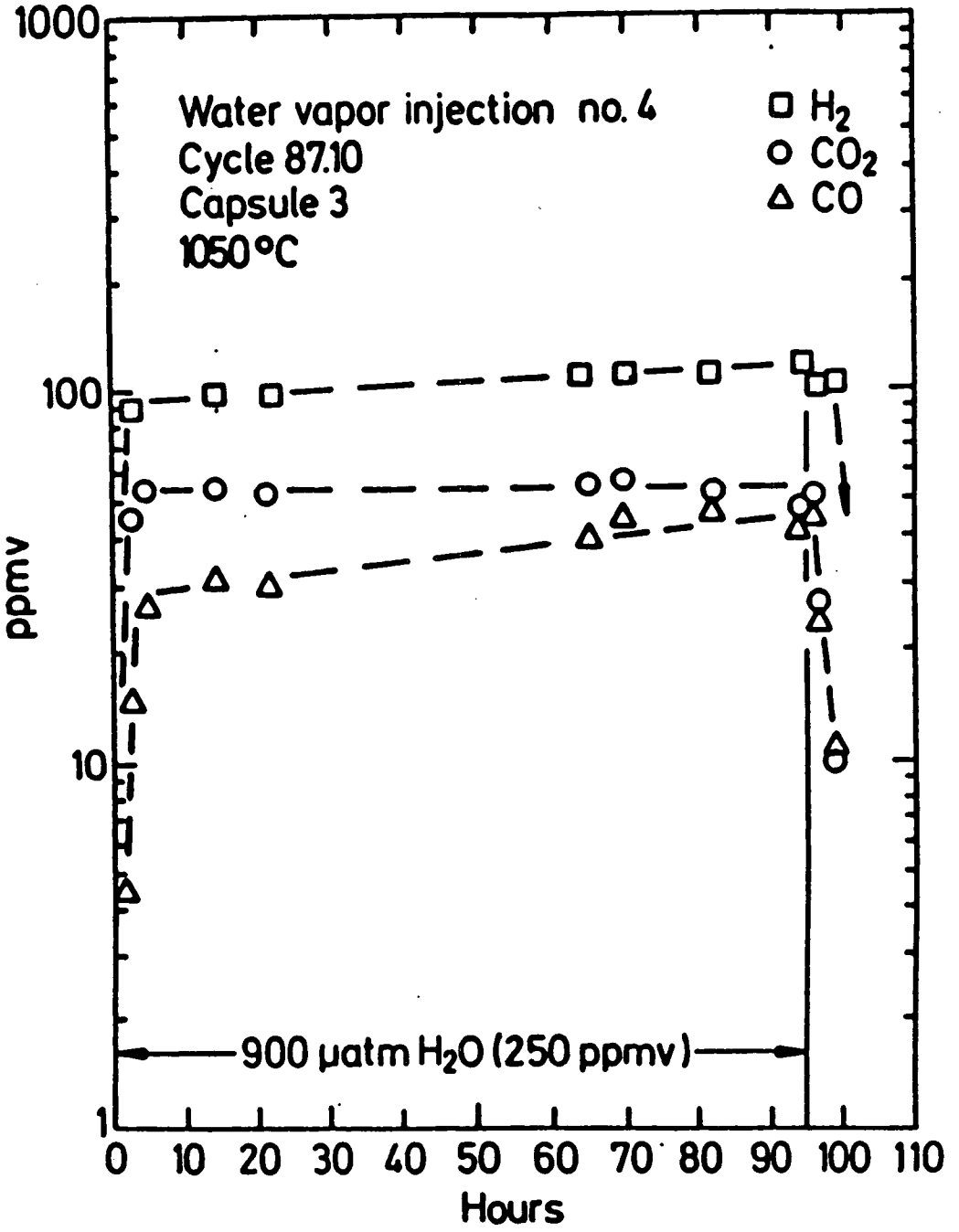

Fig. 5. Gas-impurity data during water-vapor injection No. 4. The temperature given refers to the fuel compacts. The water-vapor concentration is the inlet value. This figure is taken from Ref. 2.

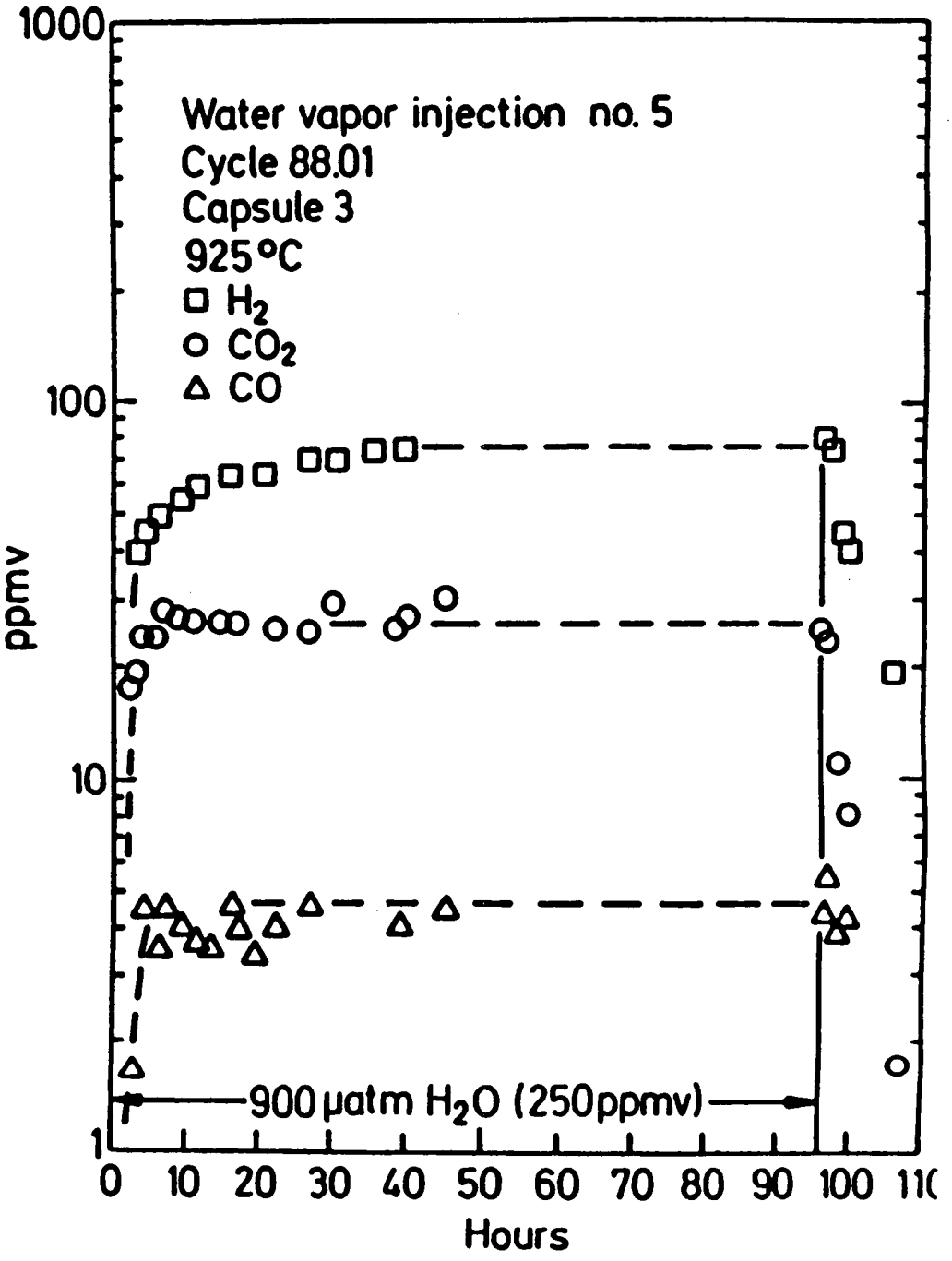

Fig. 6. Gas-impurity data during water-vapor injection No. 5. The temperature given refers to the fuel compacts. The water-vapor concentration is the inlet value. This figure is taken from Ref. 2.

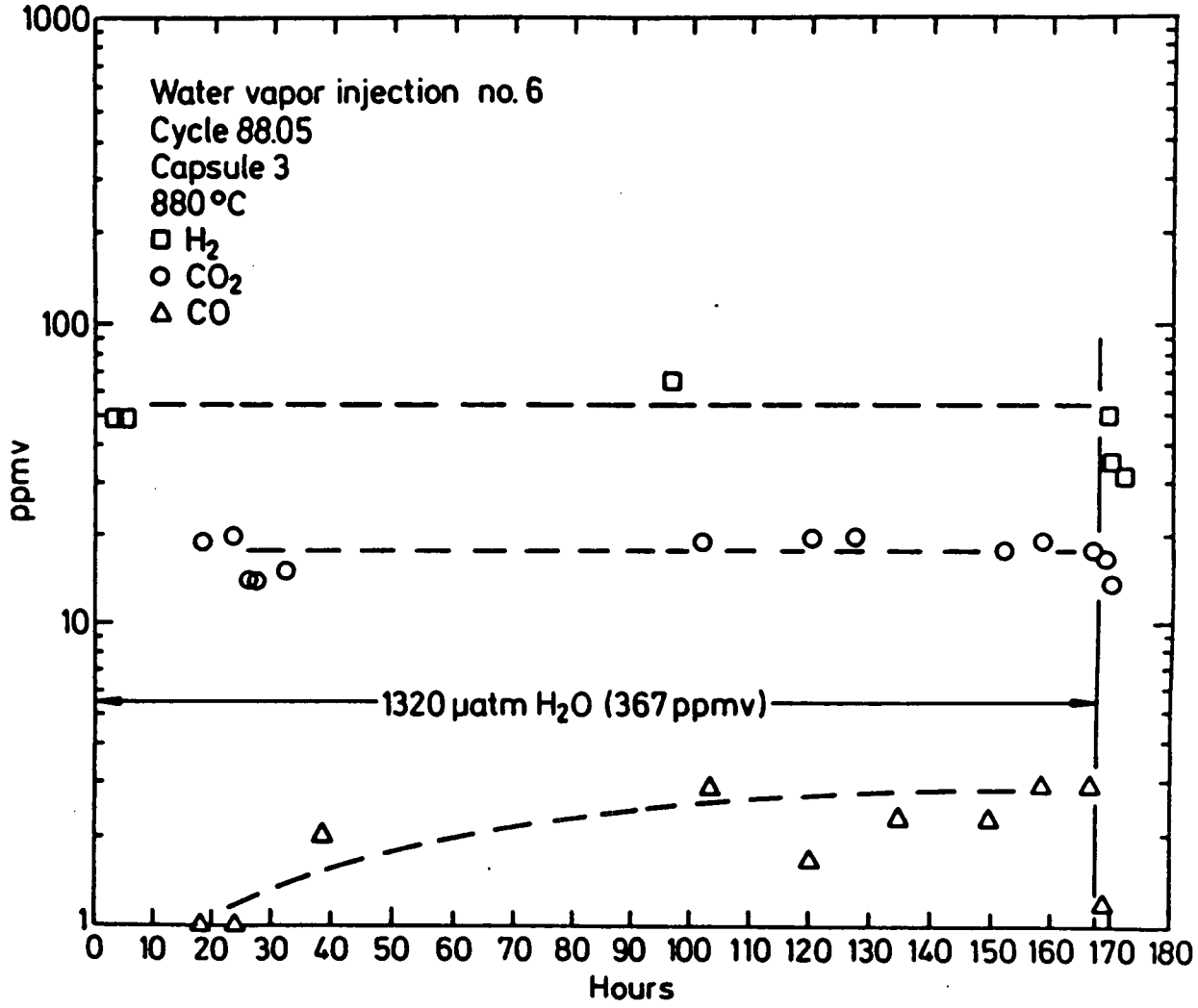

Fig. 7. Gas-impurity data during water-vapor injection No. 6. The temperature given refers to the fuel compacts. The water-vapor concentration is the inlet value. This figure is taken from Ref. 2.

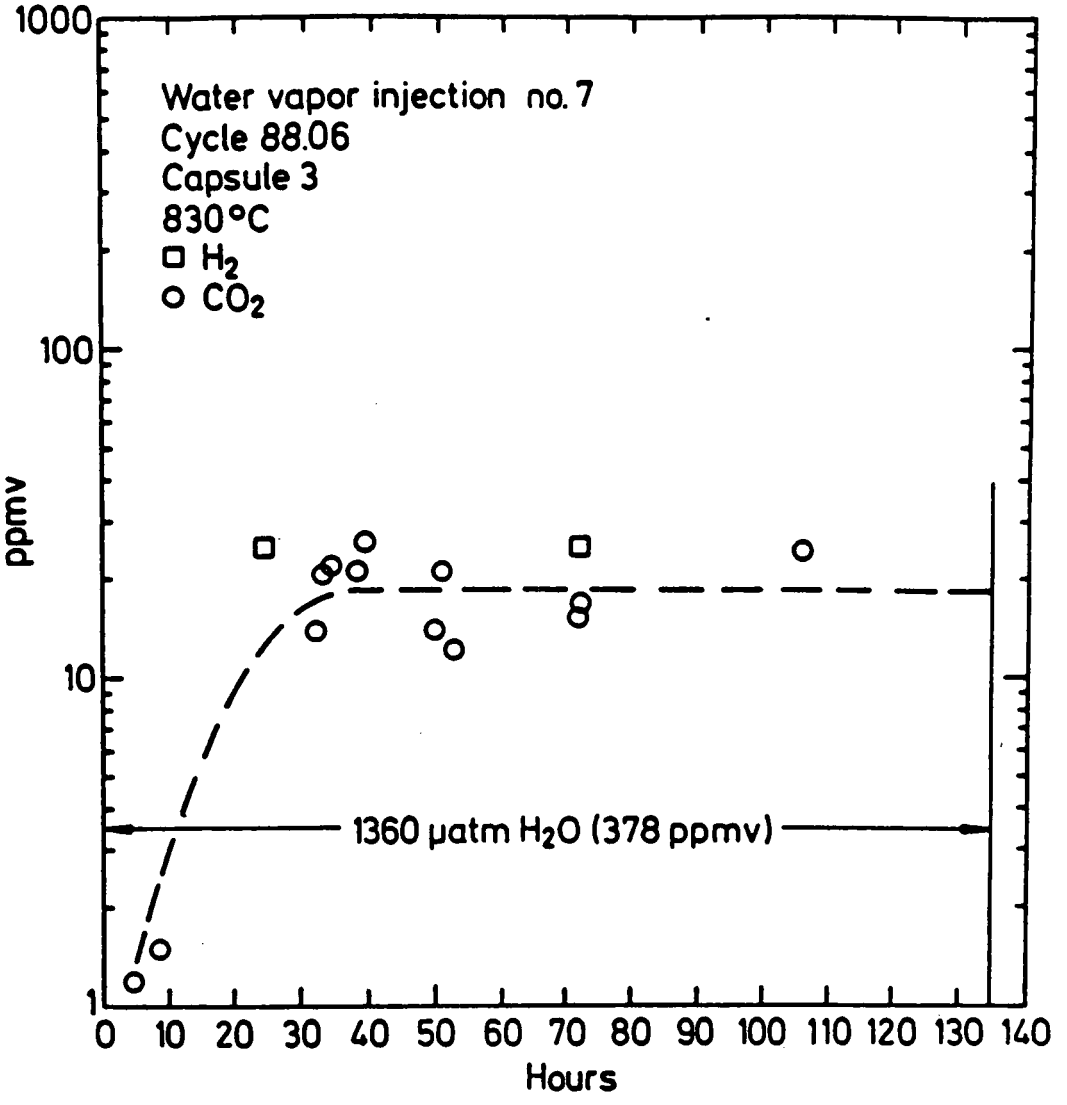

Fig. 8. Gas-impurity data during water-vapor injection No. 7. The temperature given refers to the fuel compacts. The water-vapor concentration is the inlet value. This figure is taken from Ref. 2.

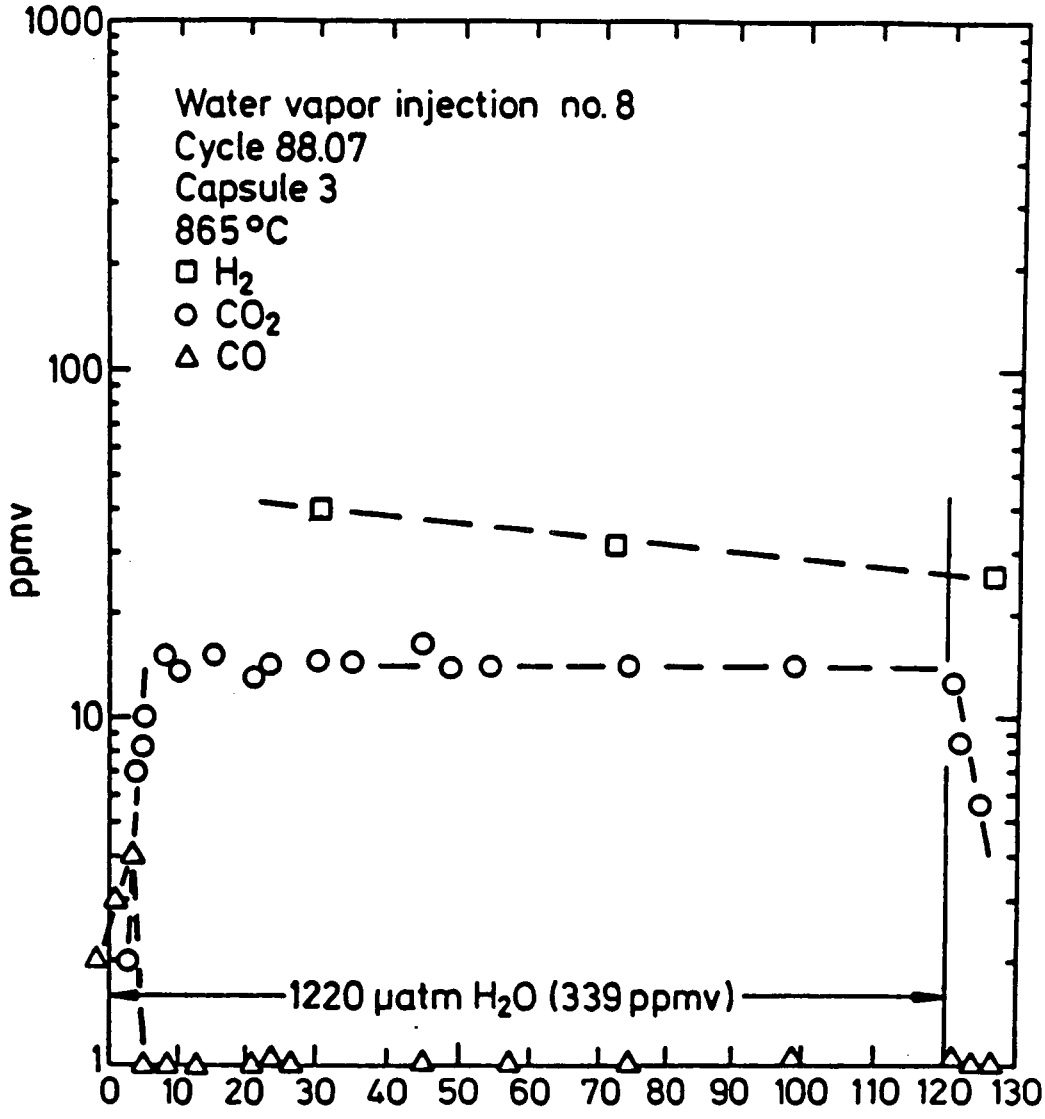

Fig. 9. Gas-impurity data during water-vapor injection No. 8. The temperature given refers to the fuel compacts. The water-vapor concentration is the inlet value. This figure is taken from Ref. 2.

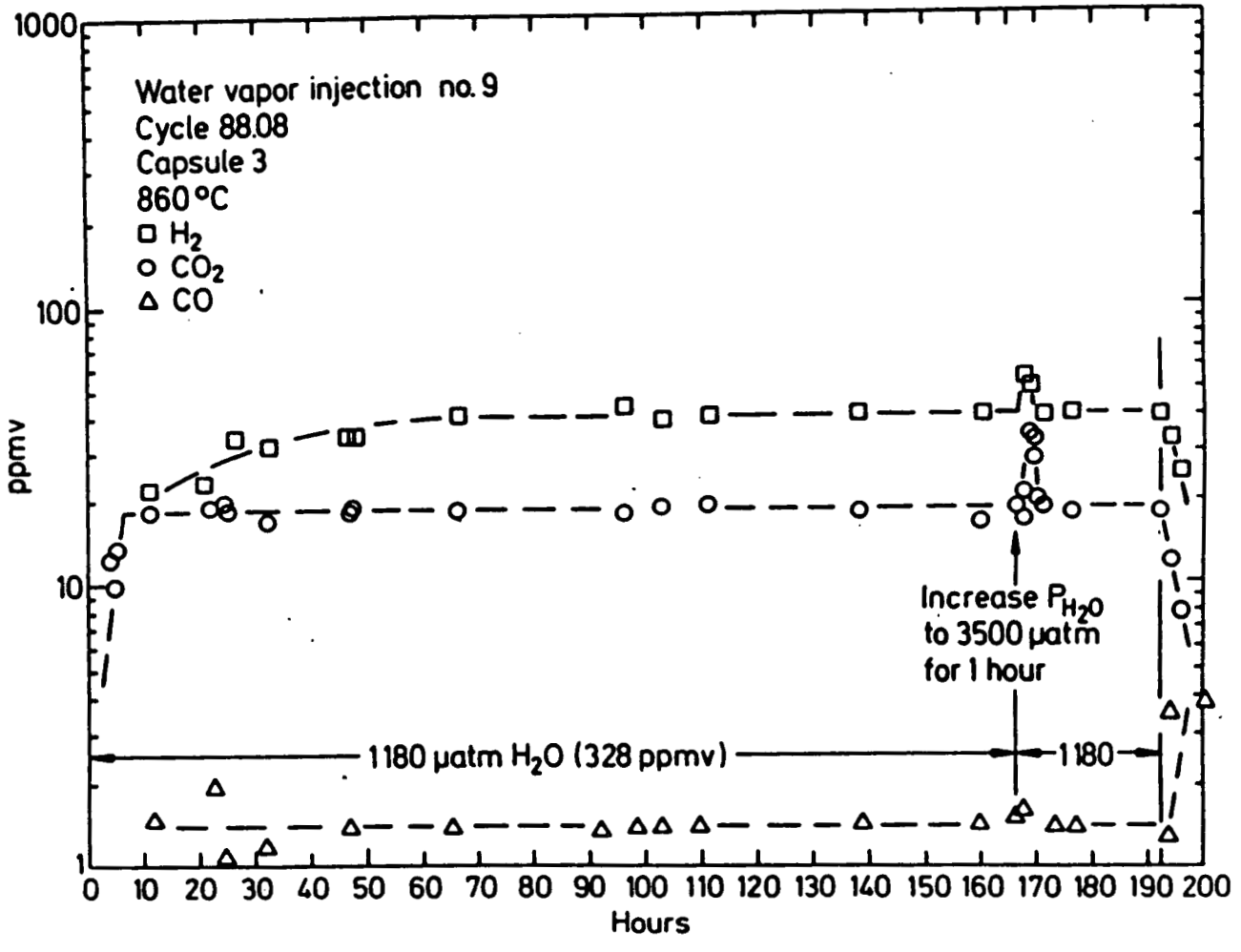

Fig. 10. Gas-impurity data during water-vapor injection No. 9. The temperature given refers to the fuel compacts. The water-vapor concentration is the inlet value. This figure is taken from Ref. 2.

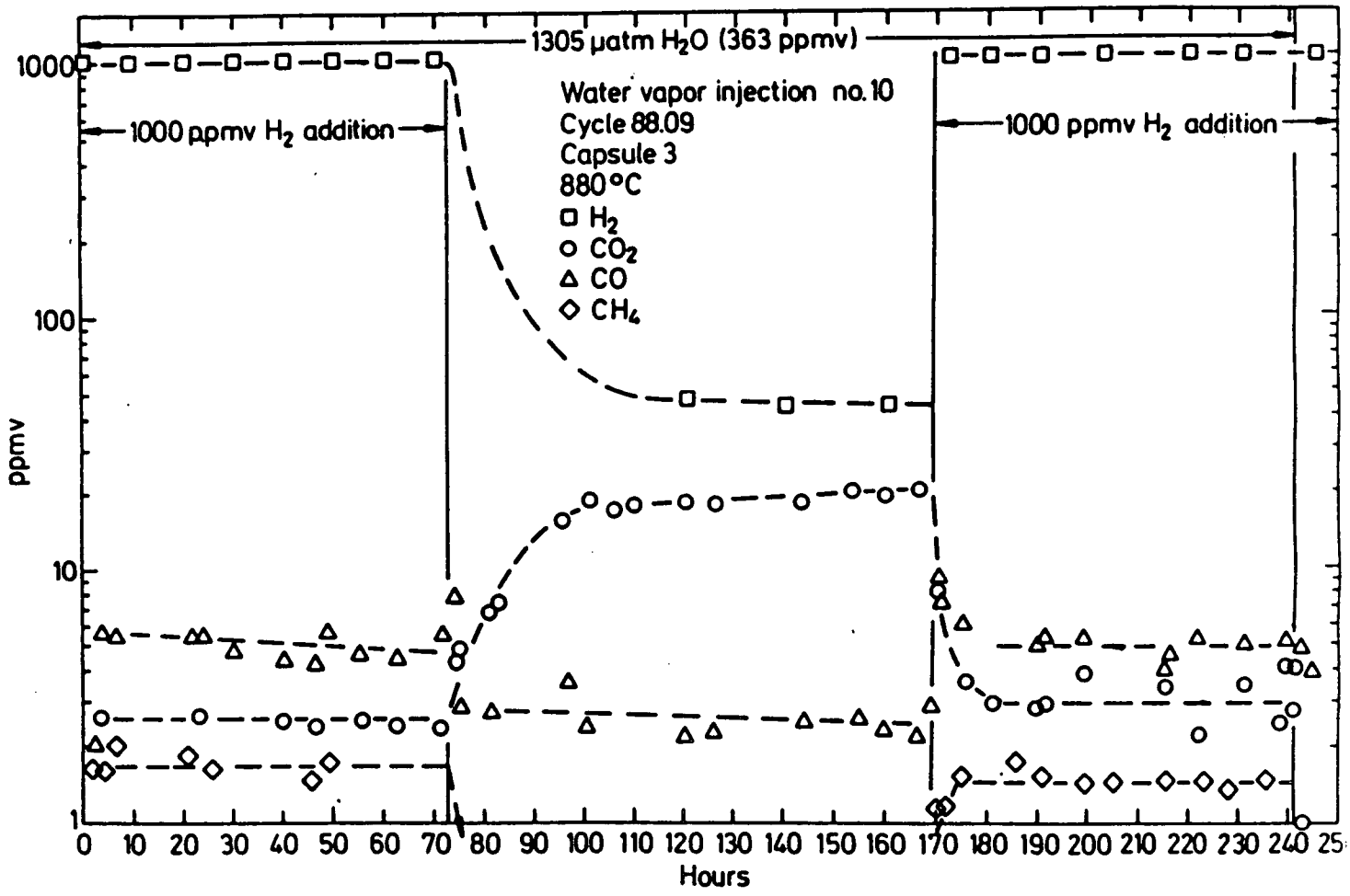

Fig. 11. Gas-impurity data during water-vapor injection No. 10. The temperature given refers to the fuel compacts. The water-vapor concentration is the inlet value. During this test hydrogen was also injected. This figure is taken from Ref. 2.

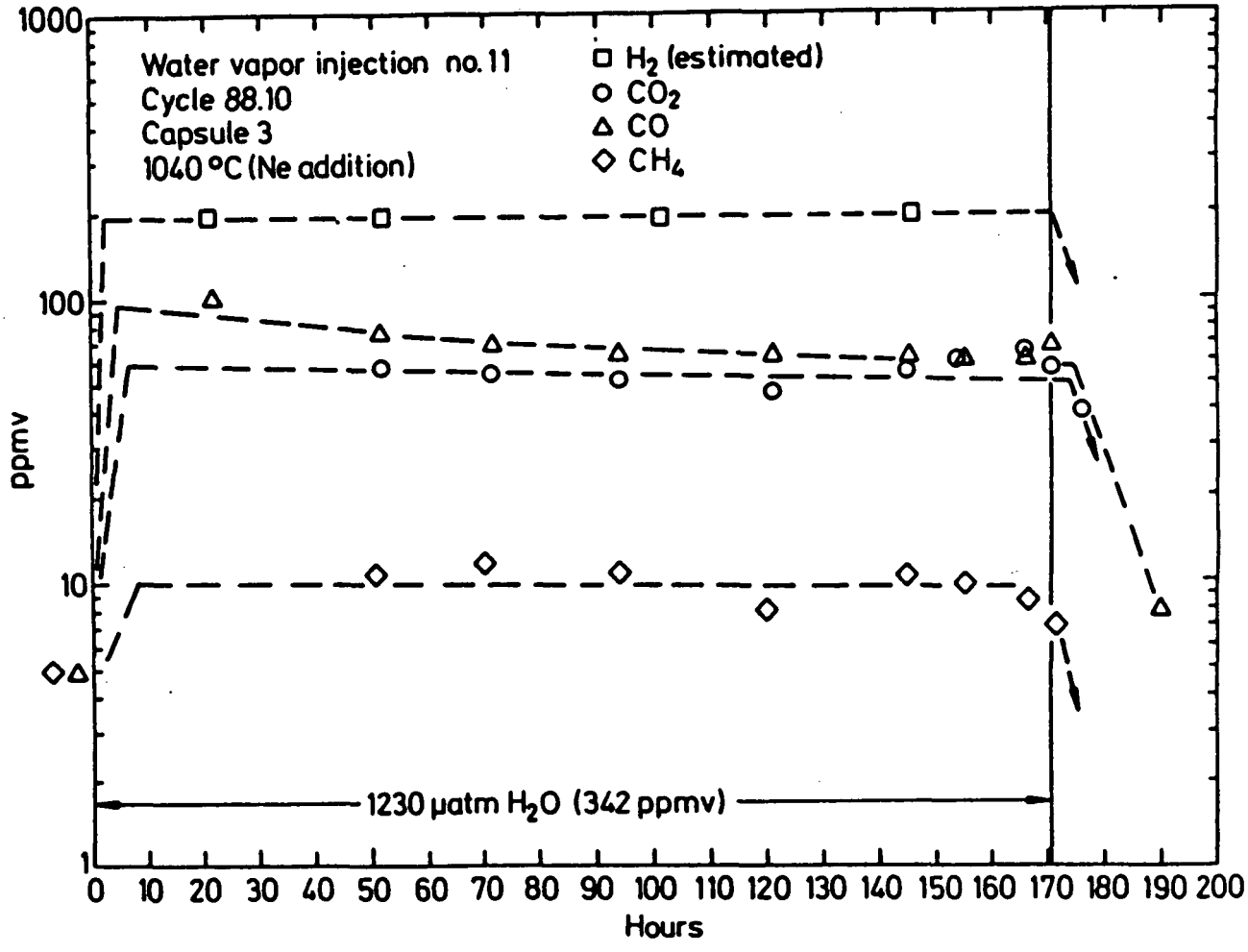

Fig. 12. Gas-impurity data during water-vapor injection No. 11. The temperature given refers to the fuel compacts. The water-vapor concentration is the inlet value. This figure is taken from Ref. 2.

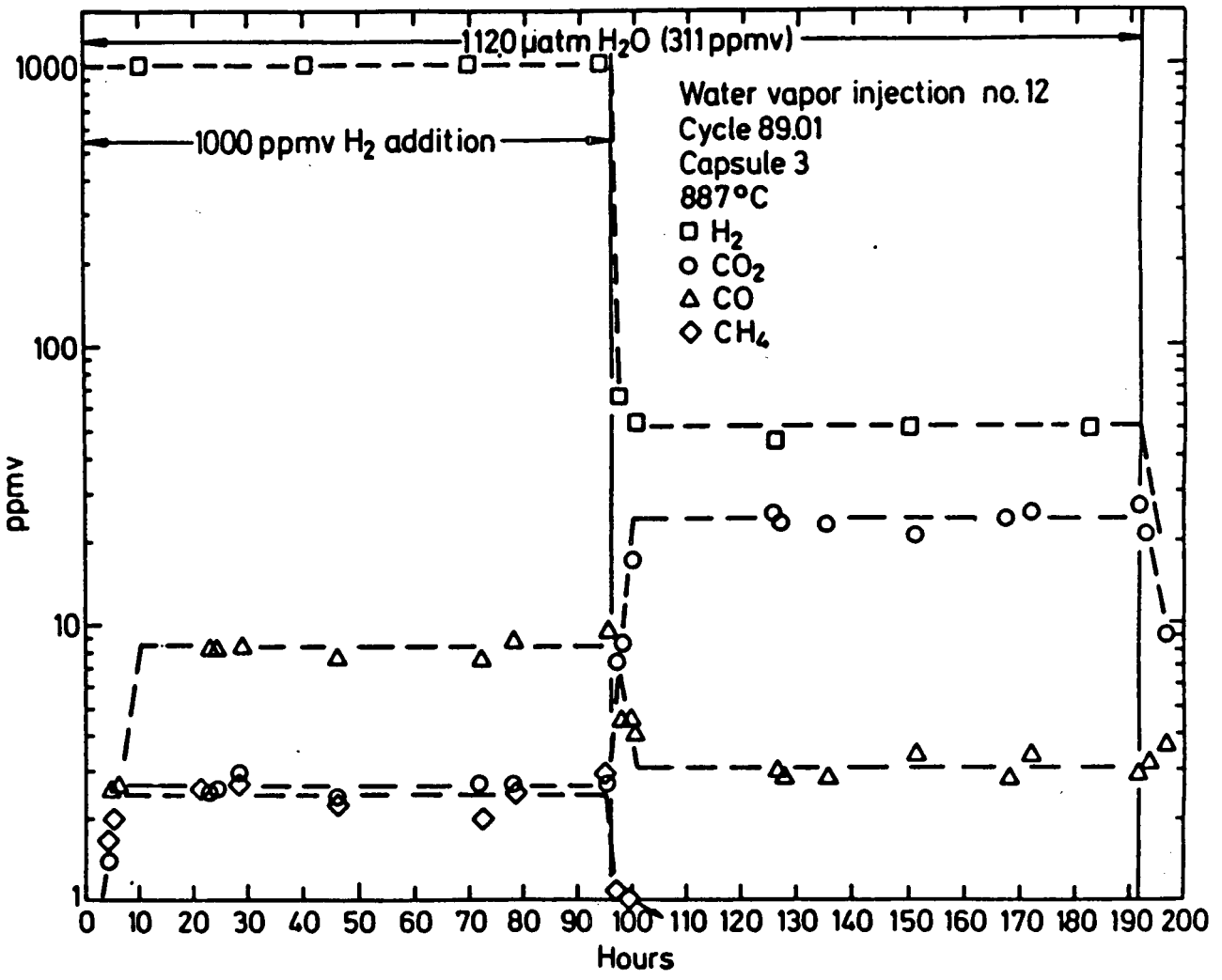

Fig. 13. Gas-impurity data during water-vapor injection No. 12. The temperature given refers to the fuel compacts. The water-vapor concentration is the inlet value. During this test hydrogen was also injected. This figure is taken from Ref. 2.

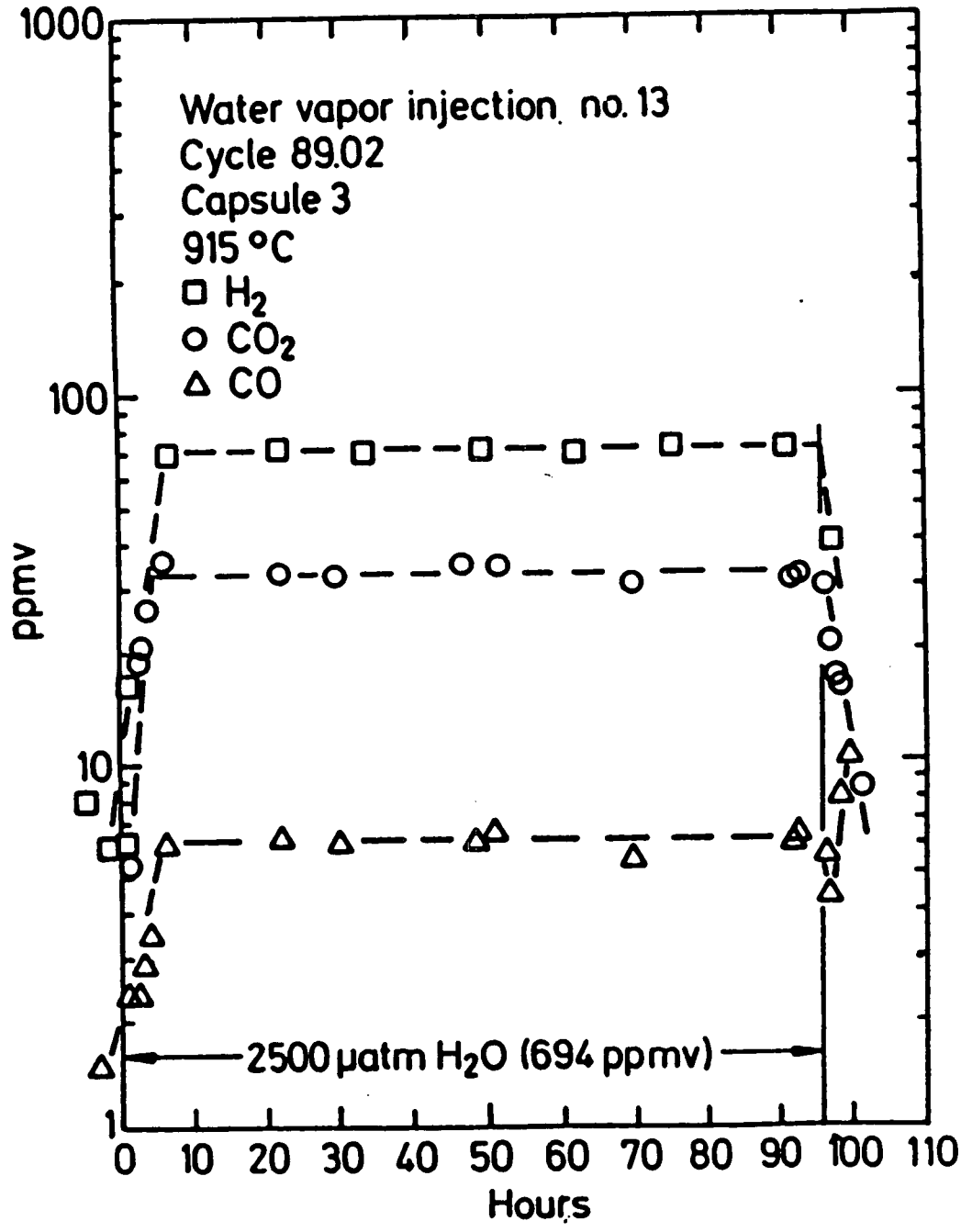

Fig. 14. Gas-impurity data during water-vapor injection No. 13. The temperature given refers to the fuel compacts. The water-vapor concentration is the inlet value. This figure is taken from Ref. 2.

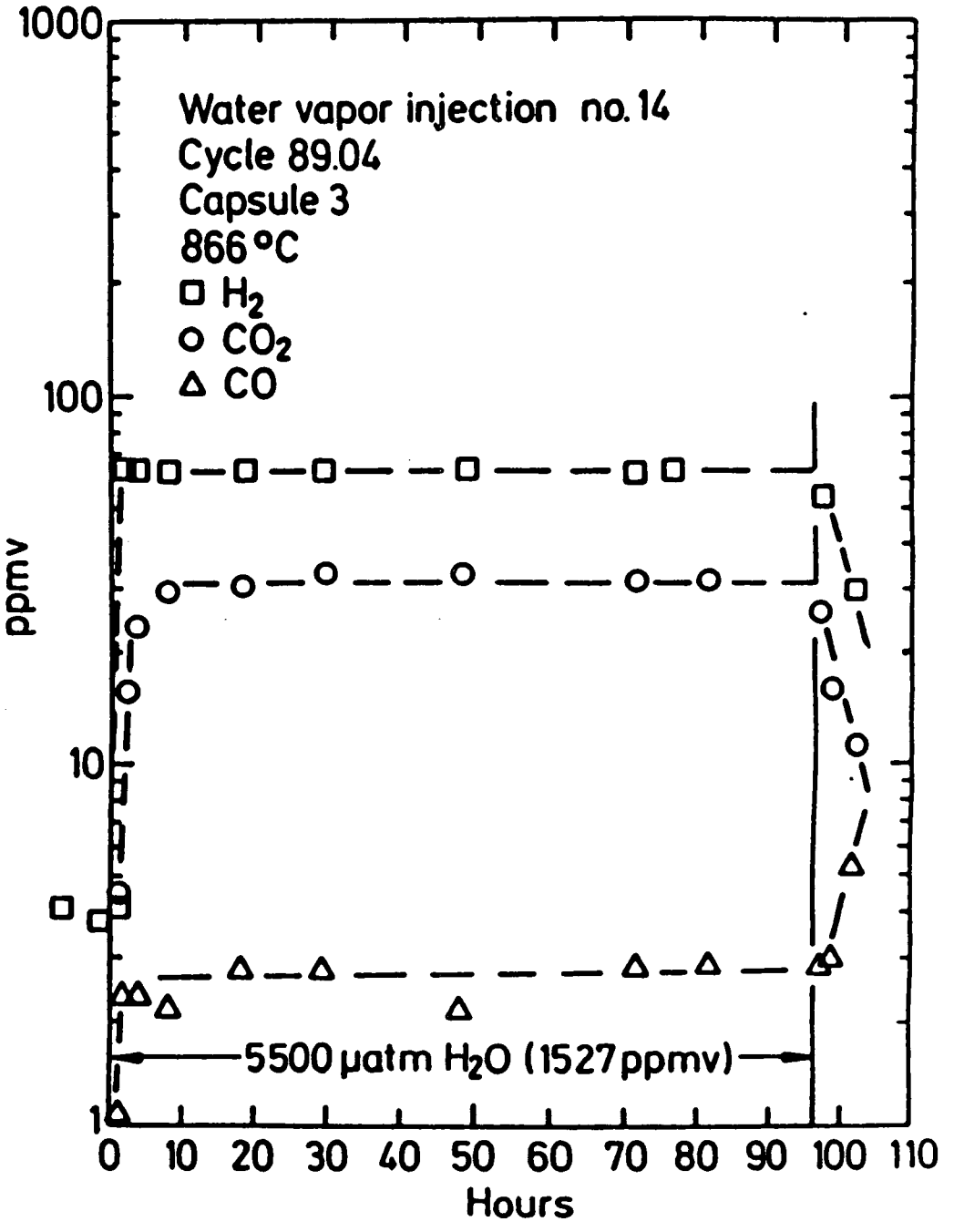

Fig. 15. Gas-impurity data during water-vapor injection No. 14. The temperature given refers to the fuel compacts. The water-vapor concentration is the inlet value. This figure is taken from Ref. 2.

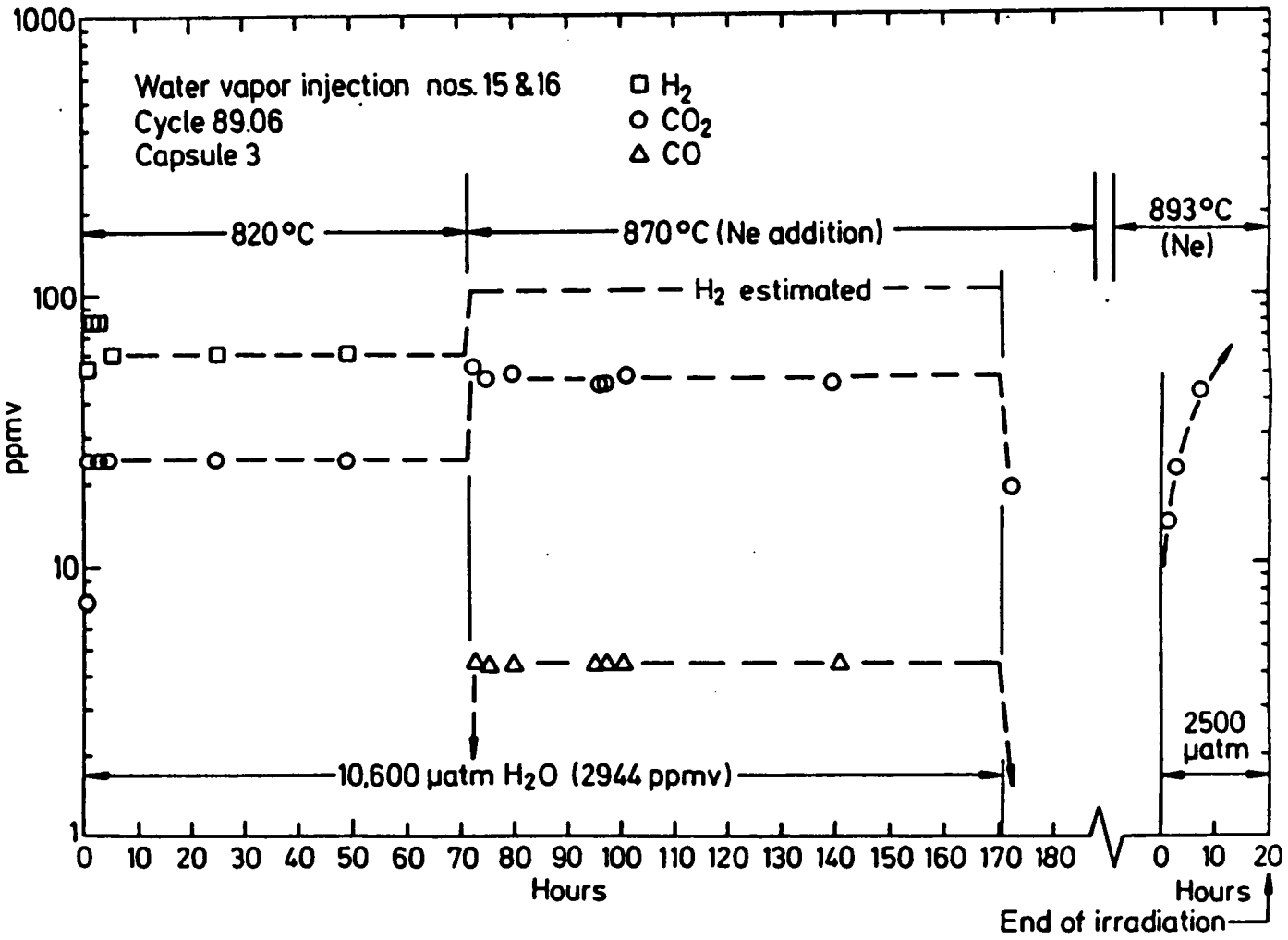

Fig. 16. Gas-impurity data during water-vapor injections Nos. 15 and 16. The temperature given refers to the fuel compacts. The water-vapor concentration is the inlet value. This figure is taken from Ref. 2.

In the sweep-gas, the water-gas-shift reaction will convert some CO to CO_2, viz.

$$CO + H_2O \rightleftarrows CO_2 + H_2 \quad . \tag{2}$$

At lower temperatures, the forward-shift reaction is thermodynamically favored. Also, because of radiolysis, the reaction rate may be higher under reactor conditions. From the reactions given by equations (1) and (2), it is apparent that 1 mole of C is consumed for every mole of (CO + CO_2) produced. The reaction of CO_2 with graphite (Boudouard reaction) will also result in some gasification. However, the CO_2-graphite reaction rate is about an order of magnitude slower than the steam-graphite reaction rate for the same conditions of temperature and gas concentrations. Also, the measured CO_2 concentrations were much smaller than the injected H_2O concentrations. Therefore, it is reasonable to neglect the Boudouard reaction in the present analysis.

A summary of the injection conditions and the calculations for converting measured concentrations of (CO + CO_2) to graphite-mass loss is given in Table 2. From Table 2, the estimated graphite-mass loss was relatively small at 0.22% of the initial mass, for the combined 2082 h in which water-vapor was injected. Table 2 also gives the numerical average of the inlet and outlet water-vapor concentrations. Despite the extremely slow sweep-gas flow rates, water-vapor depletion down the length of the capsule was relatively small during most of the injections. Therefore, graphite corrosion during the Petten experiment was not completely limited by mass-transfer effects. Hence, the data given in Table 2 for corrosion of H-451 graphite under in-pile conditions may be used for code-validation purposes.

Table 2
Oxidation Conditions and Results for Petten Experiment

	Time (h)	Graph Temp (C) (1)	H2O Press-In (Pa)	H2O Press-Ave (Pa) (2)	H2 Press-Ave (Pa)	CO Press (Pa)	CO2 Press (Pa)	Graph Loss (mg) (3)	Accum Graph Loss (mg)	Graph Loss (mass-%)
1	6	800	45	37.5	0	1.55	6.66	1.2	1.2	0
2	101	800	18	15.8	0	-	2.2	5	6.2	0
3	283	890	45	27.5	95	8.8	13.1	102	108.2	0.04
4	388	900	90	64	110	14.1	19	76	184.2	0.06
5	484	775	90	79.4	70	1.46	9.83	26	210.2	0.07
6	652	730	132	125.1	54	0.8	6.44	29	239.2	0.08
7	787	680	136	129.3	25	-	6.7	22	261.2	0.09
8	907	715	122	116.7	35	0.36	5.11	16	277.2	0.09
9	1,099	710	118	111.1	40	0.43	6.66	33	310.2	0.1
10a	1,172	730	131	128.7	1,000	1.7	0.94	4.6	314.8	0.1
10b	1,268	730	131	123.3	60	0.92	6.7	17	331.8	0.11
10c	1,340	730	131	128.7	1,000	1.8	0.9	4.7	336.5	0.11
11	1,512	890	123	91.1	177	23.4	20.2	180	516.5	0.17
12a	1,608	737	112	109.5	1,000	3	0.97	9.1	525.6	0.17
12b	1,704	737	112	102.6	50	1.1	8.8	23	548.6	0.18
13	1,800	785	250	237	70	2.2	11.9	32	580.6	0.19
14	1,896	716	550	536.2	60	1	11.27	28	608.6	0.2
15a	1,968	670	1,060	1,051	60	-	9	15.5	624.1	0.21
15b	2,067	720	1,060	1,041.6	100	1.6	17.6	45.3	669.4	0.22
16	2,082	743	250	238.1	0	-	11.9	4.3	673.7	0.22

(1) Average of the 18 thermocouples

(2) The total system pressure was 3.6 atm.

(3) Graphite-mass loss calculated from the amount of CO and CO_2 in the sweep gas exiting the capsule.

4. GRAPHITE-CORROSION PREDICTIONS

As discussed previously, the irradiation of capsule HFR-B1 provided some unique data for the validation of graphite-corrosion computer codes. In the present analysis, a simulation of graphite corrosion during the Petten experiment was performed using the REACT program. A description of the REACT corrosion models and details of the analysis are described in the following sections.

4.1. REACT COMPUTER PROGRAM

The REACT program is based on the improved corrosion model described in Ref.7 and summarized in Appendix A. Predictions obtained with REACT have shown good agreement with burnoff-profile and total burnoff measurements for unirradiated grade 2020 graphite (Ref. 7). Some of the features of REACT include:

1. A correction, from earlier corrosion models, for the mass-sink or source terms in the species-conservation equations. This correction was derived from first principles and involves dividing the uncorrected terms by the graphite void fraction, to obtain the correct units of mass of species per unit volume of pore space per unit time.

2. Inclusion of a term in the species-conservation equations, also derived from first principles, to account for the effects of gradients in void fraction (which may exist as the result of nonuniform burnoff) on transport processes.

3. Use of a numerical solution, with variable nodalization, that allows for variations of model parameters with time and spatial location.

4. Use of improved models for the burnoff factor and burnoff dependence for the effective diffusivity of steam in helium.

5. Boundary conditions that account for both transport across the boundary layer and reactions on external graphite surfaces.

4.2. MODEL GEOMETRY AND NUMERICAL SOLUTION

The graphite body (see Fig. 2) was modeled as a hollow cylinder with inner radius R_1 = 1.9 cm and outer radius R_2 = 3.1 cm. The outer radius was obtained from the actual graphite-body dimensions and the inner radius was calculated to conserve the estimated total graphite mass of 300 g. As discussed previously, the sweep gas containing the water vapor flowed in the gap space (width = 0.6 cm) between the graphite body and stainless steel shield.

A one-dimensional numerical solution was obtained for 28 nodes placed from the graphite-gas interface at $R = R_2$ to the inner radius at $R = R_1$. A fine grid was used near $R = R_2$, because of the larger gradients in water-vapor concentration near this surface. Both the nodalization and time steps were systematically varied to ensure that a stable and accurate numerical solution was being obtained. The actual node spacings and time steps may be obtained from Appendix B, which provides sample output for a representative calculation.

Obviously, the model geometry is an approximation of the actual geometry. For example, the thermocouple wells were not explicitly modeled in this analysis. However, this should not introduce significant errors since the associated volumes were small and the wells did not penetrate the complete length of the graphite body and form a

continuous gap. Also, reactions occurring within the fuel compacts were not considered in this analysis. This approximation is reasonable, since most of the corrosion will occur at high temperatures, when little water vapor will penetrate through the region between the sweep gas and fuel compacts (width $\simeq$ 0.5 cm). However, at lower temperatures, there may be a significant contribution to the measured CO and CO_2 concentrations from reactions with fuel-compact material.

Although a simplified, one-dimensional calculation was performed, the actual corrosion will vary in all three spatial directions. Around the circumference, most of the corrosion will occur near the fuel compacts where temperatures are higher. In these regions, gradients in burnoff in the radial direction are expected to be much larger than gradients in burnoff in the circumferential direction. There will also be variations in corrosion in the axial direction, caused primarily by depletion of water vapor from the sweep-gas flow down the length of the graphite body. However, water-vapor depletion was not large, particularly at the higher water-vapor concentrations, so that use of an average water-vapor concentration should not introduce significant errors into the analysis. Hence, an approximate, one-dimensional calculation is justified.

4.3. MODEL PARAMETERS

The model parameters required for the REACT program are described in Appendix A. The numerical values used in the present analysis are given below:

$\rho_{C,o}$ = graphite density = 1.77 g/cm^3 ,

$A_{BET,o}$ = BET surface area = 10^4 cm^2/g ,

ψ_o = structural parameter used to calculate the burnoff factor = 20 .

In the above symbols, the subscript o indicates the initial or unreacted value. Pressure gradients across the graphite body were assumed to be negligibly small, so that the approximation Pe = 0 was used, where Pe is the Peclet number.

Another parameter that significantly affects the graphite corrosion is the graphite temperature. The initial predictions were obtained using the graphite temperatures given in Table 2, which are a numerical average of all 18 thermocouples. When these temperatures were used, the predicted corrosion was about a factor of 2 higher than the measured values. Since the gasification rate was jointly controlled by in-pore diffusion and chemical kinetics, an intrinsic reaction rate that was a actor of $2^2 = 4$ lower would result in much better agreement with the data. This result was verified by performing calculations using a multiplier of 0.25 on the intrinsic reaction rate. It was noted that nearly the same effect would result if the absolute graphite temperatures were lowered by 5% from the thermocouple-averaged values. From Fig. 2, it can be seen that the thermocouples were located in the hotter regions around the fuel compacts, so it is expected that the actual average graphite temperatures will be somewhat lower than the thermocouple-averaged values. Also, the thermocouples in the regions between the fuel compacts and sweep-gas flow typically read about 5% lower than the thermocouples located interior to the fuel compacts. For example, during injection No. 11 thermocouple 43 measured 1199 K but thermocouple 46 measured 1139 K. As will be shown later, most of the corrosion occurred in the web region between the fuel compacts and sweep-gas flow. There may also be some localized cooling caused by the endothemic steam-graphite reaction. Therefore, it is reasonable to use graphite temperatures that are somewhat lower than the thermocouple-averaged values.

4.4. RESULTS

Figure 17 shows a comparison of model predictions for total burnoff with the experimental data. As discussed in the previous section, the predictions were obtained using more representative graphite temperatures that were 5% lower than the thermocouple-averaged temperatures. Except for the time period 650-1350 h (water-vapor injections 6-10), the model predictions agree remarkably well with the data. During this time period, the model underpredicts the data, with the difference being about 30% at 1350 h. As indicated by the change in slope of the burnoff versus time curve, graphite temperatures were lower during this time period (see Table 2). The data indicate a greater generation rate of CO and CO_2 than can be inferred from the model predictions of graphite corrosion. Two explanations can be given for this behavior. First, radiolysis may be enhancing the gasification rate. The effects of radiolysis will be more apparent at lower temperatures, when thermal reaction rates are low. The correlation for the steam-graphite reaction rate does not account for radiolysis, since the reaction rates were not measured in a radiation environment. However, if radiolysis were the primary cause for the disagreement, then it is expected that the model should underpredict the data after 1350 h since temperatures are first increased and then decreased again after this time.

A second and more likely cause for the disagreement is that there may be an additional source of CO and CO_2, other than graphite corrosion, during this time period. Figure 18 shows the predicted water-vapor concentration as a function of depth into the graphite for injection No. 7 (thermocouple-averaged temperature = 680°C) and injection No. 11 (thermocouple-averaged temperature = 890°C). From Fig. 18, it is apparent that at lower temperatures significant amounts of water vapor will penetrate the graphite to reach the fuel compacts. Potential sources for CO and CO_2 in the fuel compacts are reactions with matrix material, graphite-shim particles, pyrocarbon coatings, and the UC_2

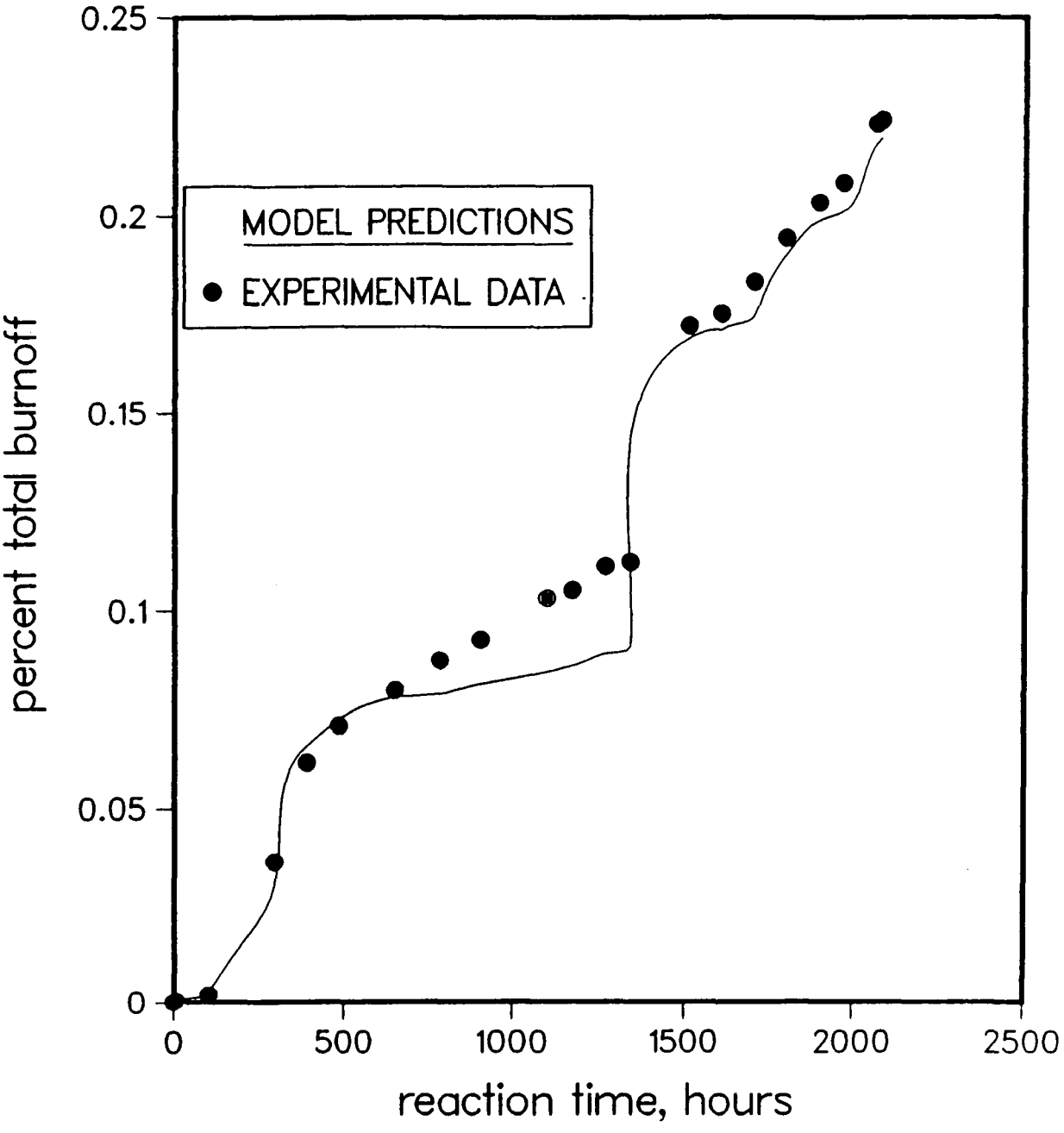

Fig. 17. Comparison of REACT predictions with the HFR-B1 graphite-corrosion data. The predictions were obtained for $\psi_o = 20$, $A_{BET,o} = 10^4$ cm^2/g, $\rho_{C,o} = 1.77$ g/cm^3, $\epsilon_o = 0.217$, $\phi = \epsilon^3$, and Pe = 0 (see Appendix A for symbol definition). The experimental conditions are given in Table 2. The graphite temperatures were assumed to be 5% lower than the thermocouple-averaged values, to account for the slightly cooler-than-average graphite in the high-corrosion regions.

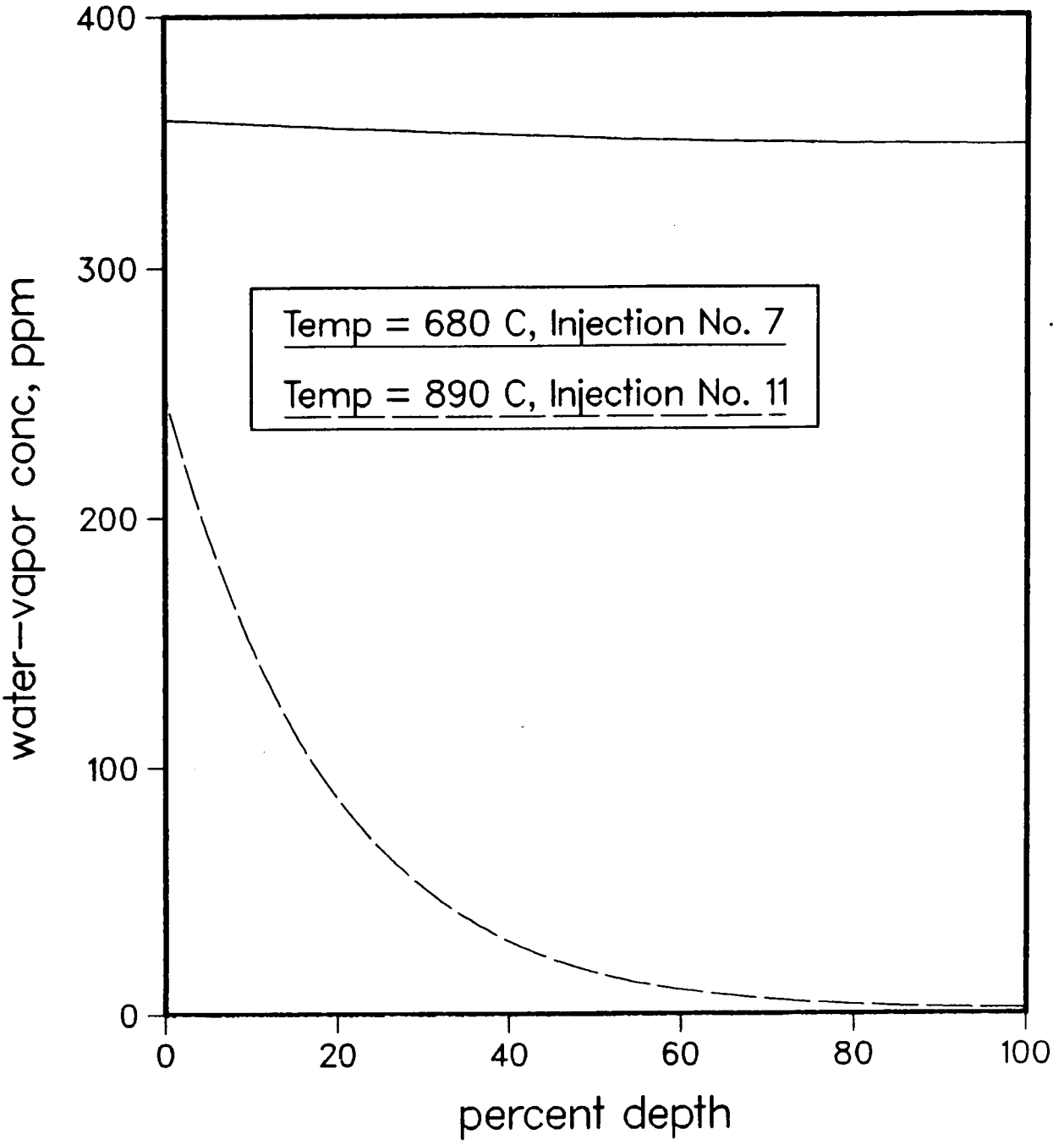

Fig. 18. REACT predictions for water-vapor concentrations as a function of depth from the graphite-gas interface. At high temperatures, water vapor is significantly depleted before reaching the fuel compacts.

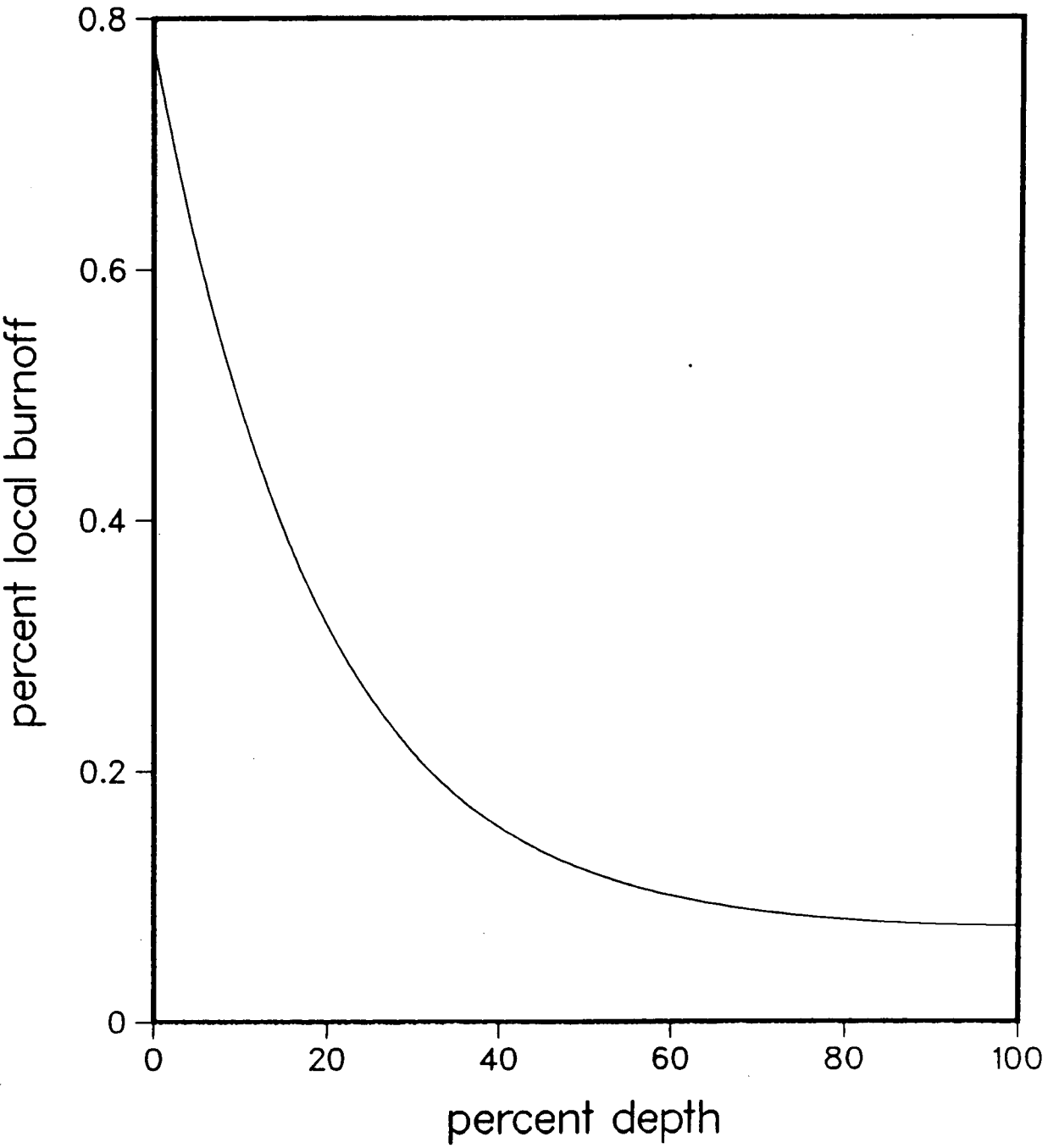

Fig. 19. REACT predictions for the percent burnoff as a function of depth from the graphite-gas interface following the final water-vapor injection. Note that most of the corrosion occurs near the graphite-gas interface, where temperatures are slightly lower than the average of thermocouple readings.

phase of exposed UCO fuel kernels. During the time period 650-1350 h, approximately 130 mg of carbon was reacted. Although the reaction rate of UC_2 with water vapor is much higher than the steam-graphite reaction rate, there are only about 4 mg of carbon in dtf particles in capsule 3. Hence, fuel hydrolysis is not the primary additional source of CO and CO_2. The most likely source is reactions with matrix material, which is normally about 10-20 times more reactive than H-451 graphite. For the HFR-B1 compacts, the matrix material may have been even more reactive, since the iron content was about a factor of 5 higher than the design value. Also, reaction rates within the fuel compacts will be higher because of the higher temperatures and possibly because of catalysis caused by fission metals such as barium or strontium.

At later times, temperatures were also lower, but an additional source of CO and CO_2 is not apparent in the data. This suggests that this source may have been completely consumed during the reaction-time period 650-1350 h. A possible source may be a highly reactive component of the matrix material.

Figure 19 shows the predicted burnoff profile as a function of depth into the graphite after the final water-vapor injection. The local burnoff is less than 1% at the surface exposed to the sweep gas and most of the burnoff occurs near this surface. Because of the low burnoff, it will probably not be useful to measure the burnoff profile during the PIE.

5. CONCLUSIONS

Based on the present analysis, it appears that the currently used correlation for the reaction of H-451 graphite with steam may be used to accurately predict in-pile graphite corrosion. The Petten data have been extremely valuable for the validation of the improved graphite-corrosion model in REACT. The data should prove to be even more valuable for validation of an integrated graphite-corrosion and fuel-hydrolysis model. The small discrepancies between model predictions and the Petten data are likely caused by reactions occurring within the fuel compacts, which were not considered in the present analysis. Additional developmental work should be performed to add a fuel-compact model to REACT.

Because of the low burnoffs achieved during the test, the Petten data are not very useful for validation of the in-pore diffusion and burnoff-factor models in REACT. These models were successfully validated in the analyses described in Ref. 7, but not under in-pile conditions. However, pre-test corrosion analyses for COMEDIE test BD-1 (Ref. 8) indicate that some useful in-pile data for burnoff profiles should result from the PIE of the reflector element.

6. REFERENCES

1. Hudritsch, W. W., V. Jovanovic, and D. L. Georghiou, "SURVEY - A Computer Code for the Thermal and Fuel Performance Analysis of High-Temperature Gas-cooled Reactors - User's Manual," GA-C17554, General Atomics, San Diego, California, March 1984.

2. Peroomian, M. B., A. W. Barsell, and J. C. Saeger, "OXIDE-3: A computer Code for Analysis of HTGR Steam or Air Ingress Accidents," GA-A12493, General Atomics, San Diego, California, January 1974.

3. Giberson, R. L. and C. A. Oster, "Computer Calculation of Reactor Graphite Oxidation," BNWL-331, Batelle Pacific Northwest Laboratory, Richland, Washington, April 1967.

4. Myers, B. F., "The Effect of Water Vapor on the Release of Gaseous Fission Products from HTGR Fuel Compacts Containing Exposed UCO Fuel (Draft)," ORNL-6610, Oak Ridge National Laboratory, Oak Ridge, Tennessee, July 1990.

5. Conrad, R., R. D. Burnette, and Th. Timke, "Irradiation of GA HTGR Fuel Rods at Real Time Simulating Operating Conditions in the HFR Petten" Rev. 0, Technical Memorandum HFR/903082, Final Irradiation Report, Commission of the European Communities, Joint Research Center, Institute of Advanced Materials, HFR Division, Petten Establishment, The Netherlands, 1990.

6. "Design Data Needs Modular High-Temperature Gas-cooled Reactor," DOE-HTGR-86025, Rev. 4, General Atomics, San Diego, California, October 1989.

7. Richards, M. B., "Reaction of Nuclear-Grade Graphite with Low Concentrations of Steam in the Helium Coolant of an MHTGR," Energy, Vol. 15, No. 9, pp. 729-739, 1990.

8. Hanson, D. L., "Specification for COMEDIE Test BD-1," DOE-HTGR-87095, Rev. B (Draft), General Atomics, San Diego, California, 1990.

APPENDIX A
REACT MODEL DESCRIPTION

A.1. CONSERVATION EQUATIONS

The REACT program solves a quasi-steady form of the steam-conservation equation in porous graphite for a hollow cylindrical geometry with inner radius R_1 and outer radius R_2. In nondimensional form, the species conservation equations are given by (Ref. 1)

$$[Pe_K - (\Phi/\epsilon)(\partial\epsilon/\partial r)](\partial Y_K/\partial r) - (1/r)\partial[(r\Phi)\partial Y_K/\partial r]/\partial r - [Da_K - (Pe_K/\epsilon)(\partial\epsilon/\partial r)]Y_K = 0 \quad , \tag{A-1}$$

where Y_K = pore-volume-averaged mass fraction of species K with K = H_2O for steam and $r = R/R_2$ is a nondimensional radial coordinate. The parameters appearing in Eq. A-1 are defined according to

$$Pe_K = R_2 v_D/\phi_o D_K \quad , \tag{A-2}$$

$$\Phi = \phi/\phi_o \quad , \tag{A-3}$$

$$Da_K = (R_2^2 F_b F_c k/\phi_o D_K) m_K (W_K/W_C)(\rho_C/\rho)/(\epsilon Y_K) \quad , \tag{A-4}$$

with v_D = Darcy velocity (cm/s),

ϕ = tortuosity coefficient, with the subscript o identifying the unreacted value,

D_K = diffusion coefficient for species K (cm^2/s),

F_b = burnoff factor,

F_c = catalysis factor,

k = intrinsic reaction rate (s^{-1}),

m_K = stoichiometry coefficient = -1 for K = H_2O (mol K/mol C),

W_K = molecular weight of species K with W_C = 12 for graphite (g of K/mol),

ρ_C = apparent graphite density (g of C/cm^3 pore + solid space),

ρ = mass-average density of gases in the pores (g of gas mixture/cm^3 pore space),

ϵ = void fraction (cm^3 pore space/cm^3 pore + solid space).

The parameter Φ measures the ratio of the local tortuosity coefficient to the unreacted value ϕ_o and Pe_K is a Peclet number that measures the ratio of convection to diffusion velocities. The product $Da_K Y_K$ is Damköhler's second similarity group and measures the ratio of composition changes produced by chemical reactions to composition changes produced by diffusion.

A.2. MODEL PARAMETERS

The intrinsic reaction rate k is given by the Langmuir-Hinshelwood relation

$$k = C_1 p_{H_2O} / (1 + C_2 p_{H_2}^{\alpha} + C_3 p_{H_2O}) \quad , \tag{A-5}$$

where p_K is the partial pressure of species K, which is expressed in terms of mass fraction according to

$$p_K = p(W/W_K) Y_K \quad , \tag{A-6}$$

where p = total pressure and W = average molecular weight $\simeq 4$ for low concentrations of steam in helium. For H-451 graphite, the constants in Eq. A-5 are given by (Ref. 2)

$$C_1 = 9.12 \times 10^7 \exp(-32{,}940/T) \text{ in atm}^{-1}\text{s}^{-1} \quad , \tag{A-7}$$

$$C_2 = 6.25 \times 10^5 \exp(-8980/T) \text{ in atm}^{-0.75} \quad , \tag{A-8}$$

$$C_3 = 3.04 \times 10^6 \exp(-11{,}520/T) \text{ in atm}^{-1} \quad , \tag{A-9}$$

$$\alpha = 0.75 \quad , \tag{A-10}$$

where T is in K.

The burnoff factor F_b is modeled according to (Ref. 3)

$$F_b = [1 - \psi_o \ln(1-b)]^{0.5} \quad , \tag{A-11}$$

where b = local fractional burnoff and ψ_o is a structural parameter defined according to

$$\psi_o = 4\pi(1-\epsilon_o)\lambda_o/(\rho_{C,o}A_{BET,o})^2 \quad . \tag{A-12}$$

In Eq. A-12, λ_o = effective pore length per unit volume and A_{BET} = BET surface area = area of pore surface per unit mass of solid. Again, the subscript o identifies the initial or unreacted state. For nuclear-grade graphite, typical values for ψ_o are in the range 20 to 70.

The diffusion coefficient for steam in helium is calculated according to

$$D_K = 1.06 \times 10^{-4}\ T^{1.58}/p \text{ in } cm^2/s \quad , \tag{A-13}$$

where T is K and p is in atm. The tortuosity coefficient ϕ is modeled according to

$$\phi = \epsilon^3 \quad , \tag{A-14}$$

which shows good agreement with measured values.

Since the burnoff dependencies for the viscous permeability and slip coefficient are not accurately known, the Peclet number Pe_K is currently treated as a constant. This approximation may be easily improved if more accurate data become available to model convective transport.

The local fractional burnoff is defined according to

$$b = 1 - \rho_C/\rho_{C,o} \quad , \tag{A-15}$$

with the time dependence of ρ_C given by

$$d\rho_C/dt = -k\rho_C \quad . \tag{A-16}$$

The void fraction ϵ is given in terms of b according to

$$\epsilon = \epsilon_o + b(1-\epsilon_o) \quad . \tag{A-17}$$

A.3. BOUNDARY CONDITIONS

If the graphite-coolant interface is at $R = R_1$, the boundary condition is

$$-\phi\partial Y_K/\partial r = (Sh/2r_o)(Y_{K,c} - Y_K) \text{ at } r = r_o \quad , \tag{A-18}$$

where Sh = Sherwood number, $r_o = R_1/R_2$, and the subscript c identifies the coolant channel. If the graphite-coolant interface is at $R = R_2$, the boundary condition is

$$\phi\partial Y_K/\partial r = Sh(R_2/D_h)(Y_{K,c} - Y_K) \text{ at } r = 1, \tag{A-19}$$

where D_h = hydraulic diameter for flow over the outer radius R_2. In principle, a term to account for heterogeneous conversions at the graphite-gas interfaces should be added to the rhs of Eqs. A-18 and A-19. This effect may be approximately accounted for by adjusting the reaction frequency as follows: $k \rightarrow k(A_t/A_p)$, where A_t is the total-surface area and A_p is the pore-surface area. For the numerical solution, this adjustment takes the form

$$k_i \rightarrow k_i(1 + A_{si}/V_i\rho_{C,o}A_{BET,o}) \quad , \tag{A-20}$$

where A_{si} = surface area of node i exposed to steam and V_i = volume of node i. Initially, this adjustment is applied only to the surface node. When the graphite in a nodal volume is completely gasified, surface

ablation has occurred and the reaction-rate adjustment is then applied to the adjacent volume.

Zero-gradient boundary conditions are assumed at the other graphite boundaries, viz.

$$\partial Y_K/\partial r = 0 \text{ at } r = 1 \text{ for flow over } R_1 \quad , \tag{A-21}$$

$$\partial Y_K/\partial r = 0 \text{ at } r = r_o \text{ for flow over } R_2 \quad .$$

A.4. NUMERICAL SOLUTION

The REACT program uses a finite-difference method to solve the coupled Eqs. A-1 and A-16 subject to the boundary conditions described in the previous section. A semi-implicit method is used to linearize the difference equations and multiple iterations within a single time step may be specified by the program user. The diffusivities at node interfaces are estimated by using a geometric mean and a donor-cell method is used to difference the first-derivative term in Eq. A-1.

APPENDIX B

Sample REACT Output

REACT - ANALYSIS OF GRAPHITE CORROSION BY STEAM IN CYLINDRICAL GEOMETRY

THE FOLLOWING IS AN ECHO OF THE INPUT FILE

```
PETTEN BURNOFF PROFILE DATA
H-451 RATE CONSTANTS
CATALYSIS FACTOR = 1.0
TORTUOSITY COEFF. = VARIABLE = VOID**3
NET DRIFT FACTOR = 1.0
BURNOFF FACTOR = VARIABLE, CAPXSI = 20.
ABET = 10000 CM**2/G
**************************************************

SPATIAL LOCATIONS (MM)
28
19.0 20.0 21.0 22.0 22.5
23.0 23.5 24.0 24.5 25.0 25.5 26.0 26.5 27.0
27.5 28.0 28.5 29.0 29.25 29.5 29.75
30.0 30.2 30.4 30.6 30.8 30.9 31.0

TIME-DEPENDENT DATA
0.0       1000. 1 9999 1019. 1019. 8.1E-4 3.6 104. 0. 0.
6.0       1000. 1 9999 1019. 1019. 8.1E-4 3.6 104. 0. 0.
6.0001    1000. 1 9999 1019. 1019. 8.1E-4 3.6  44.  0. 0.
101.       1000. 1 9999 1019. 1019. 8.1E-4 3.6  44.   0. 0.
101.0001   1000. 1 9999 1105. 1105. 7.5E-4 3.6 76.  35. 0.
111.       1000. 1 9999 1105. 1105. 7.5E-4 3.6 76.  78. 0.
121.       1000. 1 9999 1105. 1105. 7.5E-4 3.6 76.  93. 0.
141.       1000. 1 9999 1105. 1105. 7.5E-4 3.6 76. 105. 0.
293.       1000. 1 9999 1105. 1105. 7.5E-4 3.6 76. 130. 0.
293.0001   1000. 1 9999 1114. 1114. 7.4E-4 3.6 178.   5. 0.
295.       1000. 1 9999 1114. 1114. 7.4E-4 3.6 178.  90. 0.
388.       1000. 1 9999 1114. 1114. 7.4E-4 3.6 178. 110. 0.
388.0001   1000. 1 9999 996. 996. 8.3E-4 3.6 221.  10. 0.
393.       1000. 1 9999 996. 996. 8.3E-4 3.6 221.  45. 0.
400.       1000. 1 9999 996. 996. 8.3E-4 3.6 221.  58. 0.
416.       1000. 1 9999 996. 996. 8.3E-4 3.6 221.  70. 0.
428.       1000. 1 9999 996. 996. 8.3E-4 3.6 221.  75. 0.
484.       1000. 1 9999 996. 996. 8.3E-4 3.6 221. 75. 0.
484.0001   1000. 1 9999 953. 953. 8.7E-4 3.6 348.  54. 0.
652.       1000. 1 9999 953. 953. 8.7E-4 3.6 348.  54. 0.
652.0001   1000. 1 9999 905. 905. 9.1E-4 3.6 359.  25. 0.
787.       1000. 1 9999 905. 905. 9.1E-4 3.6 359.  25. 0.
787.0001   1000. 1 9999 939. 939. 8.8E-4 3.6 324.  45. 0.
907.       1000. 1 9999 939. 939. 8.8E-4 3.6 324.  25. 0.
907.0001   1000. 1 9999 934. 934. 8.9E-4 3.6 309.   9. 0.
918.       1000. 1 9999 934. 934. 8.9E-4 3.6 309.  21. 0.
937.       1000. 1 9999 934. 934. 8.9E-4 3.6 309.  31. 0.
967.       1000. 1 9999 934. 934. 8.9E-4 3.6 309.  40. 0.
1074.      1000. 1 9999 934. 934. 8.9E-4 3.6 309.  40. 0.
1074.0001  1000. 1 9999 934. 934. 8.9E-4 3.6 953.  40. 0.
1074.5     1000. 1 9999 934. 934. 8.9E-4 3.6 953.  54. 0.
1075.      1000. 1 9999 934. 934. 8.9E-4 3.6 953.  40. 0.
1075.0001  1000. 1 9999 934. 934. 8.9E-4 3.6 309.  40. 0.
1099.      1000. 1 9999 934. 934. 8.9E-4 3.6 309.  40. 0.
1099.0001  1000. 1 9999 953. 953. 8.7E-4 3.6 358. 1000. 0.
1172.       1000. 1 9999 953. 953. 8.7E-4 3.6 358. 1000. 0.
1172.0001   1000. 1 9999 953. 953. 8.7E-4 3.6 342. 1000. 0.
1181.       1000. 1 9999 953. 953. 8.7E-4 3.6 342.  300. 0.
1187.       1000. 1 9999 953. 953. 8.7E-4 3.6 342.  120. 0.
```

```
1197.       1000. 1 9999 953. 953. 8.7E-4 3.6 342.   63. 0.
1207.       1000. 1 9999 953. 953. 8.7E-4 3.6 342.   52. 0.
1214.       1000. 1 9999 953. 953. 8.7E-4 3.6 342.   48. 0.
1268.       1000. 1 9999 953. 953. 8.7E-4 3.6 342.   48. 0.
1268.0001   1000. 1 9999 953. 953. 8.7e-4 3.6 358. 1000. 0.
1340.       1000. 1 9999 953. 953. 8.7e-4 3.6 358. 1000. 0.
1340.0001   1000. 1 9999 1105. 1105. 7.5E-4 3.6 253.   10. 0.
1343.       1000. 1 9999 1105. 1105. 7.5E-4 3.6 253.  161. 0.
1512.       1000. 1 9999 1105. 1105. 7.5E-4 3.6 253.  161. 0.
1512.0001   1000. 1 9999 960. 960. 8.6E-4 3.6 304. 1000. 0.
1606.       1000. 1 9999 960. 960. 8.6E-4 3.6 304. 1000. 0.
1608.       1000. 1 9999 960. 960. 8.6E-4 3.6 285.   60. 0.
1612.       1000. 1 9999 960. 960. 8.6E-4 3.6 285.   50. 0.
1704.       1000. 1 9999 960. 960. 8.6E-4 3.6 285.   50. 0.
1704.0001   1000. 1 9999 986. 986. 8.4E-4 3.6 658.   10. 0.
1711.       1000. 1 9999 986. 986. 8.4E-4 3.6 658.   70. 0.
1800.       1000. 1 9999 986. 986. 8.4E-4 3.6 658.  70. 0.
1800.0001   1000. 1 9999 940. 940. 8.8E-4 3.6 1495.   0. 0.
1801.       1000. 1 9999 940. 940. 8.8E-4 3.6 1495.  60. 0.
1896.       1000. 1 9999 940. 940. 8.8E-4 3.6 1495.  60. 0.
1896.0001   1000. 1 9999 896. 896. 9.2E-4 3.6 2919.  46. 0.
1901.       1000. 1 9999 896. 896. 9.2E-4 3.6 2919.  50. 0.
1968.       1000. 1 9999 896. 896. 9.2E-4 3.6 2919.  50. 0.
1968.0001   1000. 1 9999 943. 943. 9.2E-4 3.6 2891. 100. 0.
2067.       1000. 1 9999 943. 943. 9.2E-4 3.6 2891. 100. 0.
2067.0001   1000. 1 9999 965. 965. 8.6E-4 3.6 661. 0. 0.
2082.0      1000. 1 9999 965. 965. 8.6E-4 3.6 661. 0. 0.

 $PARAM
 RHOC = 1.77
 ABET = 10000.0
 CAPXSI = 20.0
 GAMMA = 1.0
 EXPHI = 3.0
 FCAT = 1.0
 EXH2 = 0.75
 A1 = 9.12E+7
 A2 = 6.25E+5
 A3 = 3.06E+6
 TA1 = 32940.0
 TA2 = 8980.0
 TA3 = 11520.0
 DH = 1.2
 VARRHO = .TRUE.
 VARVD = .TRUE.
 VARPHI = .TRUE.
 VARFB = .TRUE.
 VDTRAN = .TRUE.
 SURFAC = .TRUE.
 R2FLOW = .TRUE.
 $END
```

PETTEN BURNOFF PROFILE DATA

TIME = 0.000E+00 SEC = 0.000E+00 MIN = 0.000E+00 HOURS = 0.000E+00 DAYS

A TOTAL OF 0 TIME STEPS HAVE BEEN ADVANCED

TIME PERIOD = 1
PRESSURE (ATM) = 3.6000E+00
GRAPHITE TEMPERATURE (K) = 1.0190E+03
COOLANT TEMPERATURE (K) = 1.0190E+03
COOLANT H2O CONC. (PPM) = 1.0400E+02
COOLANT H2 CONC. (PPM) = 0.0000E+00
FLOW RATE (G/S) = 8.1000E-04
PECLET NO. = 0.0000E+00
REYNOLDS NO. = 1.6708E-01
SCHMIDT NO. = 1.5810E+00
SHERWOOD NO. = 3.6600E+00

TOTAL GRAPHITE CONSUMPTION = 0.0000E+00 PERCENT
DEPTH COMPLETELY GASIFIED = 0.0000E+00 PERCENT
VOLUME COMPLETELY GASIFIED = 0.0000E+00 PERCENT

PETTEN BURNOFF PROFILE DATA

TIME = 0.000E+00 SEC = 0.000E+00 MIN = 0.000E+00 HOURS = 0.000E+00 DAYS

PROFILE DATA

NODE	LOCATION (MM)	DEPTH (PERCENT)	H2O (PPM)	BURNOFF (PERCENT)	BURNOFF FACTOR
1	1.90E+01	1.00E+02	1.04E+02	0.00E+00	1.00E+00
2	2.00E+01	9.17E+01	1.04E+02	0.00E+00	1.00E+00
3	2.10E+01	8.33E+01	1.04E+02	0.00E+00	1.00E+00
4	2.20E+01	7.50E+01	1.04E+02	0.00E+00	1.00E+00
5	2.25E+01	7.08E+01	1.04E+02	0.00E+00	1.00E+00
6	2.30E+01	6.67E+01	1.04E+02	0.00E+00	1.00E+00
7	2.35E+01	6.25E+01	1.04E+02	0.00E+00	1.00E+00
8	2.40E+01	5.83E+01	1.04E+02	0.00E+00	1.00E+00
9	2.45E+01	5.42E+01	1.04E+02	0.00E+00	1.00E+00
10	2.50E+01	5.00E+01	1.04E+02	0.00E+00	1.00E+00
11	2.55E+01	4.58E+01	1.04E+02	0.00E+00	1.00E+00
12	2.60E+01	4.17E+01	1.04E+02	0.00E+00	1.00E+00
13	2.65E+01	3.75E+01	1.04E+02	0.00E+00	1.00E+00
14	2.70E+01	3.33E+01	1.04E+02	0.00E+00	1.00E+00
15	2.75E+01	2.92E+01	1.04E+02	0.00E+00	1.00E+00
16	2.80E+01	2.50E+01	1.04E+02	0.00E+00	1.00E+00
17	2.85E+01	2.08E+01	1.04E+02	0.00E+00	1.00E+00
18	2.90E+01	1.67E+01	1.04E+02	0.00E+00	1.00E+00
19	2.93E+01	1.46E+01	1.04E+02	0.00E+00	1.00E+00
20	2.95E+01	1.25E+01	1.04E+02	0.00E+00	1.00E+00
21	2.98E+01	1.04E+01	1.04E+02	0.00E+00	1.00E+00
22	3.00E+01	8.33E+00	1.04E+02	0.00E+00	1.00E+00
23	3.02E+01	6.67E+00	1.04E+02	0.00E+00	1.00E+00
24	3.04E+01	5.00E+00	1.04E+02	0.00E+00	1.00E+00
25	3.06E+01	3.33E+00	1.04E+02	0.00E+00	1.00E+00
26	3.08E+01	1.67E+00	1.04E+02	0.00E+00	1.00E+00
27	3.09E+01	8.33E-01	1.04E+02	0.00E+00	1.00E+00
28	3.10E+01	0.00E+00	1.04E+02	0.00E+00	1.00E+00
29	COOLANT	***	1.04E+02	***	***

PETTEN BURNOFF PROFILE DATA

TIME = 2.833E+06 SEC = 4.722E+04 MIN = 7.870E+02 HOURS = 3.279E+01 DAYS

A TOTAL OF 2846 TIME STEPS HAVE BEEN ADVANCED

TIME PERIOD = 21
PRESSURE (ATM) = 3.6000E+00
GRAPHITE TEMPERATURE (K) = 9.0500E+02
COOLANT TEMPERATURE (K) = 9.0500E+02
COOLANT H2O CONC. (PPM) = 3.5900E+02
COOLANT H2 CONC. (PPM) = 2.5000E+01
FLOW RATE (G/S) = 9.1000E-04
PECLET NO. = 0.0000E+00
REYNOLDS NO. = 2.0334E-01
SCHMIDT NO. = 1.5634E+00
SHERWOOD NO. = 3.6600E+00

TOTAL GRAPHITE CONSUMPTION = 7.8847E-02 PERCENT
DEPTH COMPLETELY GASIFIED = 0.0000E+00 PERCENT
VOLUME COMPLETELY GASIFIED = 0.0000E+00 PERCENT

PETTEN BURNOFF PROFILE DATA

TIME = 2.833E+06 SEC = 4.722E+04 MIN = 7.870E+02 HOURS = 3.279E+01 DAYS

PROFILE DATA

NODE	LOCATION (MM)	DEPTH (PERCENT)	H2O (PPM)	BURNOFF (PERCENT)	BURNOFF FACTOR
1	1.90E+01	1.00E+02	3.48E+02	1.48E-02	1.00E+00
2	2.00E+01	9.17E+01	3.49E+02	1.51E-02	1.00E+00
3	2.10E+01	8.33E+01	3.49E+02	1.60E-02	1.00E+00
4	2.20E+01	7.50E+01	3.49E+02	1.78E-02	1.00E+00
5	2.25E+01	7.08E+01	3.49E+02	1.91E-02	1.00E+00
6	2.30E+01	6.67E+01	3.50E+02	2.07E-02	1.00E+00
7	2.35E+01	6.25E+01	3.50E+02	2.28E-02	1.00E+00
8	2.40E+01	5.83E+01	3.50E+02	2.53E-02	1.00E+00
9	2.45E+01	5.42E+01	3.51E+02	2.86E-02	1.00E+00
10	2.50E+01	5.00E+01	3.51E+02	3.27E-02	1.00E+00
11	2.55E+01	4.58E+01	3.52E+02	3.78E-02	1.00E+00
12	2.60E+01	4.17E+01	3.52E+02	4.43E-02	1.00E+00
13	2.65E+01	3.75E+01	3.53E+02	5.24E-02	1.01E+00
14	2.70E+01	3.33E+01	3.53E+02	6.26E-02	1.01E+00
15	2.75E+01	2.92E+01	3.54E+02	7.55E-02	1.01E+00
16	2.80E+01	2.50E+01	3.55E+02	9.18E-02	1.01E+00
17	2.85E+01	2.08E+01	3.55E+02	1.12E-01	1.01E+00
18	2.90E+01	1.67E+01	3.56E+02	1.38E-01	1.01E+00
19	2.93E+01	1.46E+01	3.56E+02	1.54E-01	1.02E+00
20	2.95E+01	1.25E+01	3.57E+02	1.71E-01	1.02E+00
21	2.98E+01	1.04E+01	3.57E+02	1.91E-01	1.02E+00
22	3.00E+01	8.33E+00	3.57E+02	2.13E-01	1.02E+00
23	3.02E+01	6.67E+00	3.58E+02	2.32E-01	1.02E+00
24	3.04E+01	5.00E+00	3.58E+02	2.54E-01	1.03E+00
25	3.06E+01	3.33E+00	3.58E+02	2.77E-01	1.03E+00
26	3.08E+01	1.67E+00	3.59E+02	3.03E-01	1.03E+00
27	3.09E+01	8.33E-01	3.59E+02	3.16E-01	1.03E+00
28	3.10E+01	0.00E+00	3.59E+02	3.31E-01	1.03E+00
29	COOLANT	***	3.59E+02	***	***

PETTEN BURNOFF PROFILE DATA

TIME = 5.443E+06 SEC = 9.072E+04 MIN = 1.512E+03 HOURS = 6.300E+01 DAYS

A TOTAL OF 5474 TIME STEPS HAVE BEEN ADVANCED

TIME PERIOD = 47
PRESSURE (ATM) = 3.6000E+00
GRAPHITE TEMPERATURE (K) = 1.1050E+03
COOLANT TEMPERATURE (K) = 1.1050E+03
COOLANT H2O CONC. (PPM) = 2.5300E+02
COOLANT H2 CONC. (PPM) = 1.6100E+02
FLOW RATE (G/S) = 7.5000E-04
PECLET NO. = 0.0000E+00
REYNOLDS NO. = 1.4649E-01
SCHMIDT NO. = 1.5931E+00
SHERWOOD NO. = 3.6600E+00

TOTAL GRAPHITE CONSUMPTION = 1.6888E-01 PERCENT
DEPTH COMPLETELY GASIFIED = 0.0000E+00 PERCENT
VOLUME COMPLETELY GASIFIED = 0.0000E+00 PERCENT

PETTEN BURNOFF PROFILE DATA

TIME = 5.443E+06 SEC = 9.072E+04 MIN = 1.512E+03 HOURS = 6.300E+01 DAYS

PROFILE DATA

NODE	LOCATION (MM)	DEPTH (PERCENT)	H2O (PPM)	BURNOFF (PERCENT)	BURNOFF FACTOR
1	1.90E+01	1.00E+02	3.19E+00	3.05E-02	1.00E+00
2	2.00E+01	9.17E+01	3.49E+00	3.12E-02	1.00E+00
3	2.10E+01	8.33E+01	4.45E+00	3.35E-02	1.00E+00
4	2.20E+01	7.50E+01	6.20E+00	3.76E-02	1.00E+00
5	2.25E+01	7.08E+01	7.49E+00	4.07E-02	1.00E+00
6	2.30E+01	6.67E+01	9.11E+00	4.46E-02	1.00E+00
7	2.35E+01	6.25E+01	1.11E+01	4.95E-02	1.00E+00
8	2.40E+01	5.83E+01	1.37E+01	5.55E-02	1.01E+00
9	2.45E+01	5.42E+01	1.68E+01	6.31E-02	1.01E+00
10	2.50E+01	5.00E+01	2.06E+01	7.24E-02	1.01E+00
11	2.55E+01	4.58E+01	2.54E+01	8.41E-02	1.01E+00
12	2.60E+01	4.17E+01	3.13E+01	9.86E-02	1.01E+00
13	2.65E+01	3.75E+01	3.86E+01	1.17E-01	1.01E+00
14	2.70E+01	3.33E+01	4.75E+01	1.39E-01	1.01E+00
15	2.75E+01	2.92E+01	5.85E+01	1.67E-01	1.02E+00
16	2.80E+01	2.50E+01	7.21E+01	2.02E-01	1.02E+00
17	2.85E+01	2.08E+01	8.88E+01	2.45E-01	1.02E+00
18	2.90E+01	1.67E+01	1.09E+02	2.99E-01	1.03E+00
19	2.93E+01	1.46E+01	1.21E+02	3.31E-01	1.03E+00
20	2.95E+01	1.25E+01	1.35E+02	3.66E-01	1.04E+00
21	2.98E+01	1.04E+01	1.49E+02	4.06E-01	1.04E+00
22	3.00E+01	8.33E+00	1.66E+02	4.50E-01	1.04E+00
23	3.02E+01	6.67E+00	1.80E+02	4.89E-01	1.05E+00
24	3.04E+01	5.00E+00	1.95E+02	5.31E-01	1.05E+00
25	3.06E+01	3.33E+00	2.12E+02	5.78E-01	1.06E+00
26	3.08E+01	1.67E+00	2.30E+02	6.28E-01	1.06E+00
27	3.09E+01	8.33E-01	2.39E+02	6.55E-01	1.06E+00
28	3.10E+01	0.00E+00	2.49E+02	6.83E-01	1.07E+00
29	COOLANT	***	2.53E+02	***	***

PETTEN BURNOFF PROFILE DATA

TIME = 7.495E+06 SEC = 1.249E+05 MIN = 2.082E+03 HOURS = 8.675E+01 DAYS

A TOTAL OF 7539 TIME STEPS HAVE BEEN ADVANCED

TIME PERIOD = 65
PRESSURE (ATM) = 3.6000E+00
GRAPHITE TEMPERATURE (K) = 9.6500E+02
COOLANT TEMPERATURE (K) = 9.6500E+02
COOLANT H2O CONC. (PPM) = 6.6100E+02
COOLANT H2 CONC. (PPM) = 0.0000E+00
FLOW RATE (G/S) = 8.6000E-04
PECLET NO. = 0.0000E+00
REYNOLDS NO. = 1.8403E-01
SCHMIDT NO. = 1.5729E+00
SHERWOOD NO. = 3.6600E+00

TOTAL GRAPHITE CONSUMPTION = 2.1960E-01 PERCENT
DEPTH COMPLETELY GASIFIED = 0.0000E+00 PERCENT
VOLUME COMPLETELY GASIFIED = 0.0000E+00 PERCENT

REACT - ANALYSIS OF GRAPHITE CORROSION BY STEAM IN CYLINDRICAL GEOMETRY

PETTEN BURNOFF PROFILE DATA

TIME = 7.495E+06 SEC = 1.249E+05 MIN = 2.082E+03 HOURS = 8.675E+01 DAYS

PROFILE DATA

NODE	LOCATION (MM)	DEPTH (PERCENT)	H2O (PPM)	BURNOFF (PERCENT)	BURNOFF FACTOR
1	1.90E+01	1.00E+02	5.12E+02	7.66E-02	1.01E+00
2	2.00E+01	9.17E+01	5.13E+02	7.74E-02	1.01E+00
3	2.10E+01	8.33E+01	5.16E+02	7.99E-02	1.01E+00
4	2.20E+01	7.50E+01	5.22E+02	8.45E-02	1.01E+00
5	2.25E+01	7.08E+01	5.25E+02	8.79E-02	1.01E+00
6	2.30E+01	6.67E+01	5.29E+02	9.20E-02	1.01E+00
7	2.35E+01	6.25E+01	5.34E+02	9.72E-02	1.01E+00
8	2.40E+01	5.83E+01	5.39E+02	1.04E-01	1.01E+00
9	2.45E+01	5.42E+01	5.44E+02	1.12E-01	1.01E+00
10	2.50E+01	5.00E+01	5.50E+02	1.21E-01	1.01E+00
11	2.55E+01	4.58E+01	5.57E+02	1.34E-01	1.01E+00
12	2.60E+01	4.17E+01	5.64E+02	1.49E-01	1.01E+00
13	2.65E+01	3.75E+01	5.71E+02	1.67E-01	1.02E+00
14	2.70E+01	3.33E+01	5.79E+02	1.90E-01	1.02E+00
15	2.75E+01	2.92E+01	5.88E+02	2.19E-01	1.02E+00
16	2.80E+01	2.50E+01	5.97E+02	2.55E-01	1.03E+00
17	2.85E+01	2.08E+01	6.06E+02	2.99E-01	1.03E+00
18	2.90E+01	1.67E+01	6.16E+02	3.54E-01	1.03E+00
19	2.93E+01	1.46E+01	6.21E+02	3.86E-01	1.04E+00
20	2.95E+01	1.25E+01	6.26E+02	4.22E-01	1.04E+00
21	2.98E+01	1.04E+01	6.32E+02	4.62E-01	1.05E+00
22	3.00E+01	8.33E+00	6.37E+02	5.07E-01	1.05E+00
23	3.02E+01	6.67E+00	6.42E+02	5.46E-01	1.05E+00
24	3.04E+01	5.00E+00	6.46E+02	5.89E-01	1.06E+00
25	3.06E+01	3.33E+00	6.51E+02	6.36E-01	1.06E+00
26	3.08E+01	1.67E+00	6.55E+02	6.87E-01	1.07E+00
27	3.09E+01	8.33E-01	6.58E+02	7.14E-01	1.07E+00
28	3.10E+01	0.00E+00	6.60E+02	7.43E-01	1.07E+00
29	COOLANT	***	6.61E+02	***	***